Received: 20 February 2018 | Revised: 6 July 2018 | Accepted: 26 July 2018

DOI: 10.1111/gbi.12312

ORIGINAL ARTICLE

WILEY gebiology

Morphological and isotopic changes of heterocystous cyanobacteria in response to N_2 partial pressure

Shaelyn N. Silverman[1,2] | Sebastian H. Kopf[1] | Brad M. Bebout[3] | Richard Gordon[4,5] | Sanjoy M. Som[2,3]

[1]Department of Geological Sciences, University of Colorado Boulder, Boulder, Colorado

[2]Blue Marble Space Institute of Science, Seattle, Washington

[3]Exobiology Branch, NASA Ames Research Center, Moffett Field, California

[4]Gulf Specimen Marine Laboratory & Aquarium, Panacea, Florida

[5]Department of Obstetrics and Gynecology, C. S. Mott Center for Human Growth and Development, Wayne State University, Detroit, Michigan

Correspondence
Sebastian H. Kopf, Department of Geological Sciences, University of Colorado, Boulder, CO.
Email: sebastian.kopf@colorado.edu
and
Sanjoy M. Som, Blue Marble Space Institute of Science, Seattle, WA.
Email: sanjoy@bmsis.org

Funding information
Ames Research Center; University of Colorado Boulder; National Aeronautics and Space Administration, Grant/Award Number: 80NSSC17K0667

Abstract

Earth's atmospheric composition has changed significantly over geologic time. Many redox active atmospheric constituents have left evidence of their presence, while inert constituents such as dinitrogen gas (N_2) are more elusive. In this study, we examine two potential biological indicators of atmospheric N_2: the morphological and isotopic signatures of heterocystous cyanobacteria. Biological nitrogen fixation constitutes the primary source of fixed nitrogen to the global biosphere and is catalyzed by the oxygen-sensitive enzyme nitrogenase. To protect this enzyme, some filamentous cyanobacteria restrict nitrogen fixation to microoxic cells (heterocysts) while carrying out oxygenic photosynthesis in vegetative cells. Heterocysts terminally differentiate in a pattern that is maintained as the filaments grow, and nitrogen fixation imparts a measurable isotope effect, creating two biosignatures that have previously been interrogated under modern N_2 partial pressure (pN_2) conditions. Here, we examine the effect of variable pN_2 on these biosignatures for two species of the filamentous cyanobacterium *Anabaena*. We provide the first in vivo estimate of the intrinsic isotope fractionation factor of Mo-nitrogenase (ε_{fix} = −2.71 ± 0.09‰) and show that, with decreasing pN_2, the net nitrogen isotope fractionation decreases for both species, while the heterocyst spacing decreases for *Anabaena cylindrica* and remains unchanged for *Anabaena variabilis*. These results are consistent with the nitrogen fixation mechanisms available in the two species. Application of these quantifiable effects to the geologic record may lead to new paleobarometric measurements for pN_2, ultimately contributing to a better understanding of Earth's atmospheric evolution.

KEYWORDS

air pressure, *Anabaena*, heterocyst, nitrogen fixation, nitrogen isotopes, nitrogenase

1 | INTRODUCTION

The coevolution of Earth's atmosphere and biosphere over geological time offers the possibility for microbial species to reveal a wealth of knowledge about Earth's history. The chemical composition and physical structure of Earth's ancient atmosphere are active areas of research because these properties can leave perceptible imprints on rocks (Rasmussen & Buick, 1999; Som, Catling, Harnmeijer, Polivka, & Buick, 2012; Som et al., 2016). Here, we focus on dinitrogen (N_2), a relatively inert gas due to the triple bond between nitrogen atoms, yet a crucial element for life, as nitrogen is a key component of amino acids, nucleic acids, and ATP. Several nitrogen sources and sinks control the atmospheric nitrogen concentration. The magnitudes of these fluxes are likely to have changed over geological time (Som

et al., 2016), which would have significantly affected N_2 partial pressure (pN_2) in the past. Independent methods, including paleobarometric measurements (Busigny, Cartigny, & Philippot, 2011; Som et al., 2012; Marty, Zimmerman, Pujol, Burgess, & Philippot, 2013; Som et al., 2016; Avice et al., 2018; summarized schematically in Figure 1) and modeling efforts (Barry & Hilton, 2016; Berner, 2006; Goldblatt et al., 2009; Johnson & Goldblatt, 2017, 2018; Mallik, Li, & Wiedenbeck, 2018; Stüeken, Kipp, Koehler, Schwieterman et al., 2016), have attempted to constrain pN_2 throughout Earth's history. However, these methods have yielded conflicting upper limits for early Earth pN_2, warranting the search for additional proxies. Physical markers for air pressure in the geologic record have been interrogated to reveal information about the ancient atmosphere, but are limited in usefulness because they require uncommon depositional histories. Fossil biological structures and isotopic biomarkers may hold additional clues about the atmosphere because biology responds more readily to environmental changes than geology does.

Cyanobacteria are photosynthetic oxygen-producing bacteria that have existed on Earth for at least 2.35 billion years (Ga; Kopp, Kirschvink, Hilburn, & Nash, 2005; Ward, Kirschvink, & Fischer, 2016) and possibly longer (up to 3 Ga; Buick, 2008; Planavsky et al., 2014; Eickmann et al., 2018). The onset of oxygen accumulation in our atmosphere 2.4 Ga ago, a major biogeochemical transition of the Earth surface environment commonly referred to as the Great Oxidation Event (GOE), has been linked to their ecological dominance (Kopp et al., 2005). In addition, cyanobacteria contribute the largest flux of biologically available nitrogen to Earth's ecosystems through their ability to convert N_2 to organic nitrogen through nitrogen fixation (Equation 1; Gallon, 1992).

$$N_2 + 8H^+ + 8e^- \rightarrow 2NH_3 + H_2. \quad (1)$$

This enzymatic process is believed to have arisen early in cyanobacteria, as biochemical considerations suggest a likely emergence of nitrogenase before the rise of atmospheric oxygen 2.4 Ga ago (Broda & Peschek, 1983; Fani, Gallo, & Lio, 2000; Navarro-Gonzalez, McKay, & Mvondo, 2001). Isotopic evidence points to the possible existence of this enzyme during the Archean (Beaumont & Robert, 1999; Stüeken, Buick, Guy, & Koehler, 2015).

1.1 | Heterocyst pattern

Among the multitude of cyanobacteria genera, *Anabaena* are of particular interest as potential pN_2 proxies. *Anabaena* are photosynthetic organisms that can overcome inorganically fixed nitrogen limitation in their environment through nitrogen fixation. Because nitrogenase, the enzyme responsible for nitrogen fixation, is inactivated by oxygen, *Anabaena* have evolved specialized cells known as heterocysts to protect nitrogenase during nitrogen fixation. Thus, heterocysts spatially separate the two incompatible processes that operate in *Anabaena* sp.: photosynthesis and nitrogen fixation. Nitrogenase expression and heterocyst development likely begin when photosynthetic vegetative cells become starved of bioavailable nitrogen beyond a threshold (Brown & Rutenberg, 2014; Fleming & Haselkorn, 1973; Kulasooriya, Lang, & Fay, 1972). Some vegetative cells then undergo a series of structural and biochemical changes during differentiation into heterocysts, including developing multiple envelope layers (Murry & Wolk, 1989), increasing their respiration rate (Dalton & Postgate, 1969), and degrading the photosystem II complex (Thomas, 1970), that minimize the amount of oxygen present inside the cell. After dissolution into the aqueous environment and diffusion into the vegetative cells, N_2 is believed to enter heterocysts through their terminal pores (Figure 2; Walsby, 2007). N_2 is then fixed by nitrogenase and laterally distributed to neighboring cells along the filaments (Popa et al., 2007).

Heterocysts present a substantial energy burden to the filaments, as heterocysts consume energy but do not fix carbon, and only rarely divide to yield vegetative cells that can fix carbon (Wolk, 1965). Through evolution, this energy burden has led to optimization of the location and number of heterocysts necessary in *Anabaena* species. The heterocyst frequency is therefore likely regulated in a spacing pattern to achieve the right balance between fixed nitrogen and carbon with minimal energy expenditure. Known factors that control heterocyst development and frequency include the expression of key heterocyst- and nitrogenase-specific genes, as well as the bioavailability of metals (Attridge & Rowell, 1997) and nitrogen (e.g., Golden & Yoon, 2003; Kumar, Mella-Herrera, & Golden, 2009) in the environment. Here, we investigate whether maintenance of the spaced pattern of heterocysts—that is, after the initial pattern is established—is controlled by N_2 availability. In turn, N_2 availability influences the rate of nitrogen fixation by nitrogenase. Assuming that (a) bioavailable nitrogen is completely absent in the environment, (b) a constant amount of nitrogenase is manufactured in each heterocyst, (c) vegetative cells consume fixed nitrogen at a uniform rate during growth and division, and (d) intracellular nitrogen starvation triggers heterocyst differentiation, it seems plausible that heterocyst spacing could respond to, and thus serve as a proxy for, pN_2. Considering this, we hypothesize that the distance between adjacent heterocysts along a filament is a reflection of the dissolved concentration of N_2, which is proportional to atmospheric pN_2 as described by Henry's law (Sander, 2015) when the aqueous and gaseous phases are in equilibrium.

We test the hypothesis that heterocyst spacing is a function of pN_2 with two species of filamentous cyanobacteria: *Anabaena cylindrica* and *Anabaena variabilis*. *A. cylindrica* contains a *nif1* gene cluster, which encodes a Mo-dependent nitrogenase expressed exclusively in heterocysts under oxic or anoxic growth conditions (Murry, Hallenbeck, & Benemann, 1984; Thiel, Lyons, Erker, & Ernst, 1995). As nitrogenase fixes N_2 only in the heterocysts (Figure 2), organic nitrogen should propagate along *A. cylindrica* filaments at a rate proportional to pN_2 with cells midway between heterocysts becoming starved of nitrogen as the filament lengthens. Thus, the heterocyst pattern in *A. cylindrica* should respond to pN_2. In *A. variabilis*, a second Mo-nitrogenase can be expressed in all vegetative

cells by the *nif2* gene cluster under anoxic and microoxic growth conditions (Schrautemeier, Neveling, & Schmitz, 1995; Thiel et al., 1995). Although either nitrogenase (Nif1 or Nif2) can independently satisfy the nitrogen requirements of *A. variabilis* filaments, they can be expressed simultaneously (Thiel et al., 1995), precluding a pN_2-dependent effect on heterocyst spacing.

1.2 | Nitrogen isotope fractionation

Biological processes involving different isotopes of any element may be accompanied by measurable isotope fractionation or partial separation based on mass. Nitrogen has a minor naturally occurring stable isotope (^{15}N) of one mass unit heavier than its most abundant form, ^{14}N. These isotopes have similar properties and participate in the same chemical reactions, but exhibit different reaction rates due to varying reaction kinetics and bond energies. Typically, lighter isotopes have slightly faster reaction rates in enzymatic processes, so tend to be preferentially incorporated in metabolic reactions such as carbon and nitrogen fixation, producing isotopically light biomass. The overall isotope fractionation in a metabolic process can be observed in participating reactants and products and is the result of individual enzymes' intrinsic isotope effects (e.g., by nitrogenase in the nitrogen fixation step of Figure 2) and the overall sequence, reversibility, and relative rates of all involved reaction steps (Hayes, 2004). In nitrogen fixation by cyanobacterial filaments, the most substantial isotope effect occurs at the enzymatic step of nitrogen fixation inside the heterocysts (Sra et al., 2004). However, the observable net fractionation between the resulting biomass and starting N_2 reservoir ($\varepsilon^{15}N_{Norg/N2.gas}$) is also heavily influenced by the diffusional exchange between the practically infinite reservoir of gaseous N_2 outside the filament and the active site of the nitrogenase enzyme inside the heterocysts. Thus, changes in pN_2 availability should affect the resulting isotope fractionation regardless of whether heterocysts are the only site of nitrogen fixation or whether nitrogen fixation by vegetative cells additionally plays a role. We therefore hypothesize that pN_2 is recorded within the nitrogen isotopic composition of the filaments (i.e., that $\varepsilon^{15}N_{Norg/N2.gas}$ changes in response to pN_2) and test this hypothesis in this study with both *A. variabilis* and *A. cylindrica*.

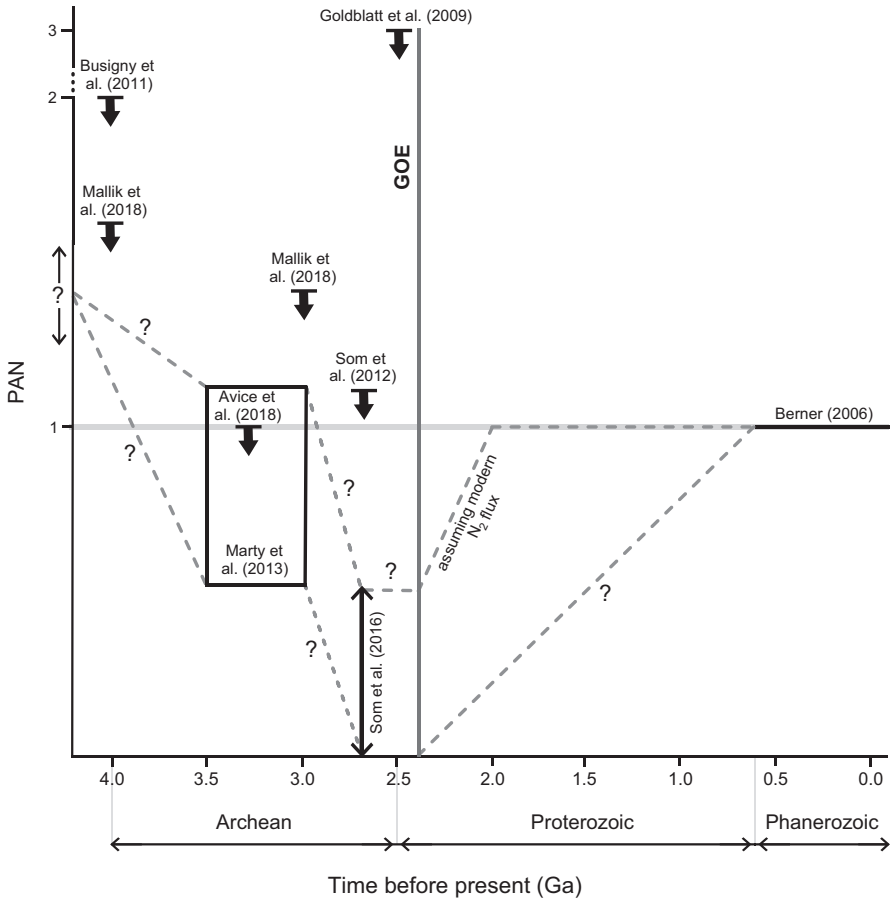

FIGURE 1 Current estimates for pN_2 throughout Earth's history, with the assumption that, during the Neoarchean, the main contributor to total atmospheric pressure was likely pN_2. Constraints are heavily data-limited, but paleobarometric measurements indicate pN_2 has fluctuated in a U-shaped trend, reaching a minimum before the Great Oxidation Event (GOE). Capped arrows denote upper limits. Graph compiled from Busigny et al. (2011), Avice et al. (2018), Marty et al. (2013), Som et al. (2012, 2016) (assuming $pN_2 \approx P_{tot}$), and Berner (2006)

2 | MATERIALS AND METHODS

2.1 | Strains and culture conditions

Stock cultures of *Anabaena cylindrica* PCC 7122 and *Anabaena variabilis* ATCC 29413 were maintained at atmospheric CO_2 in 100-ml Erlenmeyer flasks with 30 ml of nitrate-containing BG-11 medium (Rippka, Deruelles, Waterbury, Herdman, & Stanier, 1979). All experiments were inoculated at 1% v/v from ~7-day-old washed stock cultures into 10 ml of degassed, nitrate-free culture medium (BG-11_0) in 25-ml crimp-sealed anaerobic culture tubes. Media contained ~2 μM Mo and ~100 μM Fe to ensure nitrogenase was not metal-limited and was supplemented with 20 mM HEPES (pK_a = 7.5) and adjusted to pH 7.8 prior to sterilization in order to buffer against the slight acidification from CO_2 in the headspace. All stock cultures and experiments were incubated at 27°C on a cool white LED panel secured to a shaking platform agitated at 100 rpm to ensure continuous mixing and prevent localized depletion of CO_2/N_2 and/or localized buildup of O_2. The light panel was dimmed to 40–50 μE m^{-2} s^{-1} by a voltage regulating microcontroller, and the cultures were shielded from external light sources. Culture growth was measured daily by optical density at 750 nm (OD_{750}) through the anaerobic culture tubes using a Spectronic 20D+ spectrophotometer (Thermo Scientific, Waltham, MA, USA) with a culture tube adapter. The headspace of the anaerobic culture tubes was composed of 0.2 bar CO_2 (i.e., 20%), variable pN_2, and He as balance gas (1 bar total) and was controlled by initial and subsequent daily (as soon as OD_{750} > 0.1) flushing and equilibration to 1 bar with the gas mixtures. Implementation of this semicontinuous culture setup was determined based on preliminary experiments that observed pH and O_2 variation after one single headspace flushing (see Supporting Information Appendix S4 for details). CO_2 was included in the headspace at this high level to provide a virtually unlimited source of inorganic carbon and ensure that fixed nitrogen was the only limiting nutrient throughout the course of the experiments. Gas mixtures were generated using a custom-built gas blending system (Kopf Lab, University of Colorado Boulder) equipped with a digital pressure regulator and three differential pressure-based mass flow controllers (Alicat Scientific, Tucson, AZ, USA) calibrated for CO_2, N_2, and He, respectively. The headspace composition of a few cultures was confirmed using a Model 8610C gas chromatograph (SRI Instruments, Torrance, CA, USA) fitted with a 2 m long, 2 mm ID SilcoSmooth tubing packed with ShinCarbon ST 80/100 mesh stationary phase (Restek part number 80486-800, Bellefonte, PA, USA) and a thermal conductivity detector, with helium as the carrier gas. All experiments were conducted in biological triplicates or quadruplicates and included abiotic controls (medium without cells).

2.2 | Heterocyst patterns

Heterocyst patterns of culture samples were analyzed for pN_2 influence. For general heterocyst pattern analysis, 200 μl samples were withdrawn from anaerobic culture tubes either after cultures reached stationary growth phase (*A. cylindrica*, *t* = 10–15 days) or during exponential phase (*A. variabilis*, *t* = 7–10 days). For comparison of *A. cylindrica* heterocyst distances at different phases of culture growth, samples were withdrawn at early-exponential (4 days), late-exponential (7 days), and stationary (15 days) phases. Cells were then fixed with 3% paraformaldehyde in phosphate-buffered saline and stored in the refrigerator at 4°C. Heterocysts were identified by bright-field microscopy coupled with autofluorescence (Mariscal, Herrero, & Flores, 2007) using a long-pass (>615 nm) emission filter cube. Micrographs were taken on a Zeiss Axio Imager.Z1 with a 40× air objective, and images were captured with a Zeiss AxioCam MRm camera (Carl Zeiss Microscopy, Peabody, MA, USA). In addition to standard methods for visual identification of heterocysts (Yoon & Golden, 2001), lack of autofluorescence was used as an identifier for heterocysts in *Anabaena* filaments as illustrated in Figure 3. Protoheterocysts were counted as mature heterocysts in consideration that they would ultimately terminally differentiate, and intervals were quantified as the number of vegetative cells between successive heterocysts (n_{cbh}; Equation 3). Any replicating vegetative

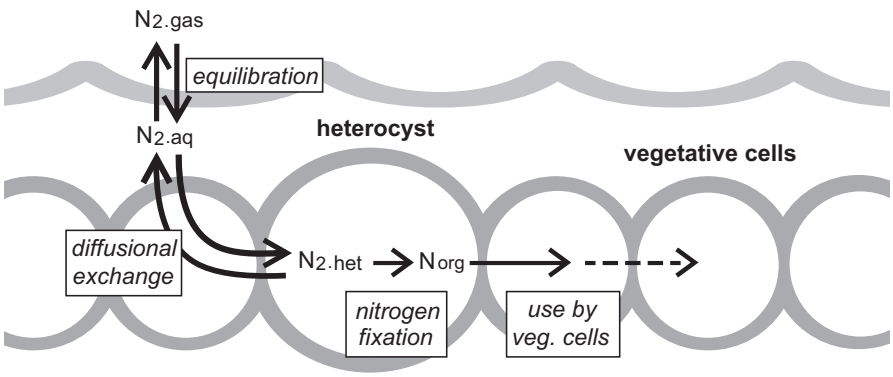

FIGURE 2 Overview schematic of the nitrogen fixation and distribution process in heterocystous cyanobacteria. At equilibrium, the concentration of N_2 gas that dissolves in the aqueous phase ($N_{2.aq}$) is proportional to the pN_2 in the atmosphere or headspace above the liquid ($N_{2.gas}$) as described by Henry's law. Dissolved N_2 diffuses into the vegetative cells and through to the heterocysts ($N_{2.het}$) where it is fixed by nitrogenase into organic nitrogen (N_{org}) and propagated to the vegetative cells. Not pictured: alternative pathway for nitrogen fixation in the vegetative cells of some heterocystous cyanobacteria (e.g., *A. variabilis*)

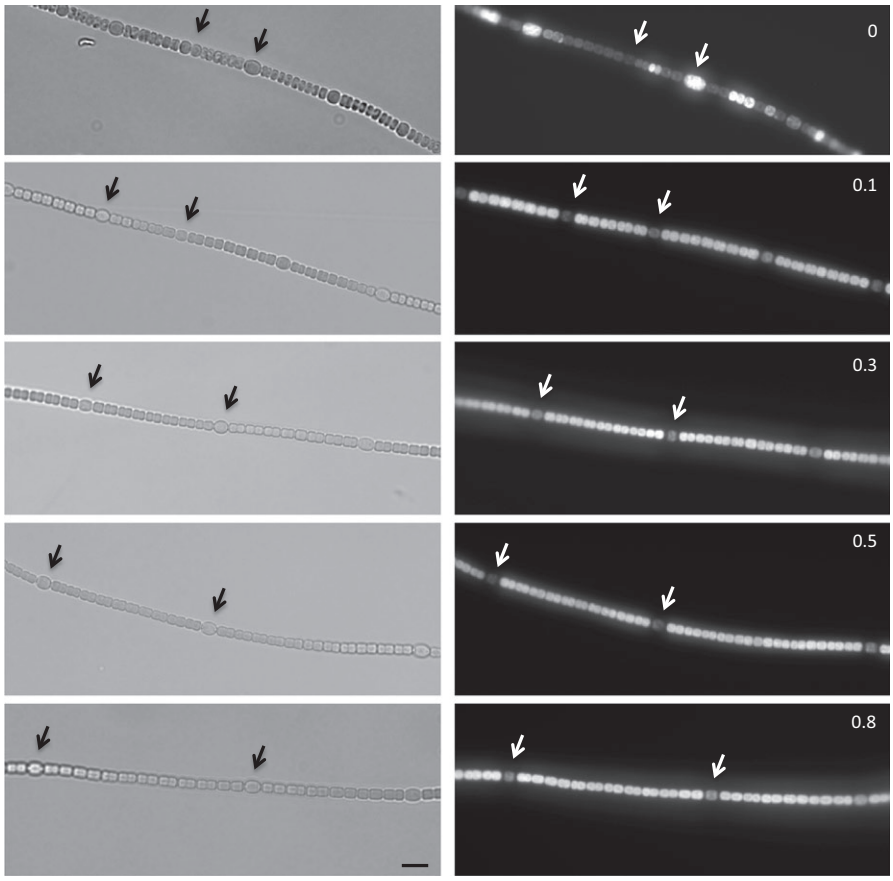

FIGURE 3 In descending order: *Anabaena cylindrica* filaments grown in nitrogen-free BG-11_0 media for 11 days under pN_2 = 0, 0.1, 0.3, 0.5, and 0.8 bar, respectively. Corresponding micrographs were taken in bright-field (left panels) and fluorescence (right panels). Mean distance between heterocysts (denoted by arrows for one representative interval) along filaments increased with pN_2. Scale bar, 10 μm

cells were counted as two individual cells as soon the septum separating them was clearly visible. The observation of some detached heterocysts indicated a possible underestimation of average interval length. Taking filament breakage into consideration, the terminal vegetative cell sequences were recorded for estimation of the minimum distances between adjacent heterocysts. All intervals on each given filament were measured, and successive intervals from the same filament were noted for future analysis of correlation. An example of how heterocyst intervals were quantified is provided in Supporting Information Figure S1. No akinetes were observed in any samples.

2.3 | Nitrogen isotope analysis

The isotopic composition of headspace N_2 ($\delta^{15}N_{N2.gas}$) was analyzed by injection into He-purged Exetainer vials (Labco, Lampeter, UK) and continuous-flow IRMS against a N_2 standard of known isotopic composition (−1.9 ± 0.3‰ vs. air N_2) using a Gasbench coupled to a Delta V Plus isotope ratio mass spectrometer (Thermo Scientific, Waltham, MA, USA). The isotopic composition of biomass nitrogen ($\delta^{15}N_{Norg}$) was measured from culture samples following standard protocols (Zhang, Sigman, Morel, & Kraepiel, 2014): Biomass was collected by vacuum filtration onto 0.8-μm glass fiber filters precombusted at 500°C, and approximately 750 μg of dry biomass from each sample was measured by EA-IRMS using a Flash 2000 elemental analyzer coupled to a Delta V Plus isotope ratio mass spectrometer (Thermo Scientific, Waltham, MA). Acetanilide (Indiana University, CAS #103-84-4) of known isotopic composition (+1.18 ± 0.02‰ and +19.56 ± 0.03‰ vs. air N_2) across a signal range from 300 μg (2.2 μmol N) to 800 μg (5.9 μmol N) was used for linearity and blank correction, and isotopic calibration. No drift corrections were necessary. Isotope abundances were recorded in the conventional δ-notation relative to air ($\delta^{15}N = [{}^{15}R_{sample}/{}^{15}R_{standard} - 1] \times 1{,}000$), where ${}^{15}R = {}^{15}N/{}^{14}N$. Data were reported as the observed fractionation factors between headspace N_2 and the resulting organic nitrogen:

$$^{15}\epsilon_{\frac{Norg}{N2.gas}} = \left[\left(\frac{^{15}N}{^{14}N}\right)_{N_{org}} / \left(\frac{^{15}N}{^{14}N}\right)_{N_{2.gas}} - 1\right] \times 1{,}000. \quad (2)$$

As is customary in the field of nitrogen isotope biogeochemistry, kinetic isotope effects in this study are defined such that normal fractionation (depletion in the light isotope) by a process has a positive epsilon ($\varepsilon > 0$). The traditional unit of ‰ (permil or parts per thousand) when used for δ and ε values in tables, text, and figures serves to indicate the customary multiplication by 1,000. The reported precision for the gaseous N_2 ($\delta^{15}N_{N2.gas}$) is based on replicate (5x) analyses of a reference standard and is estimated to be 0.045‰. The precision of the bulk organic nitrogen measurements ($\delta^{15}N_{Norg}$) is estimated to be 0.12‰ based on the maximal/most conservative analytical error predicted by the inversion of our isotope standards calibration using binomial proportion confidence

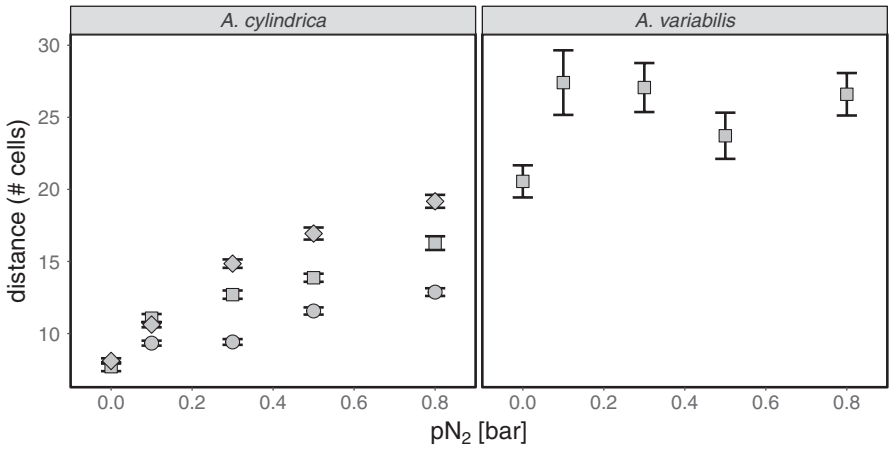

FIGURE 4 Heterocyst distances in response to pN_2. *A. cylindrica* and *A. variabilis* cultures grown in the absence of fixed nitrogen under variable pN_2 were analyzed in early-exponential (circles), late-exponential (squares), and/or stationary growth phase (diamonds). Heterocyst distances are shown as the bootstrapped mean (symbol) and error of the mean (±1 *SE*) based on at least 64 individual heterocyst intervals counted for each experimental condition (see Supporting Information Tables S1 and S3 for data summaries for *A. cylindrica* and *A. variabilis*, respectively, and Supporting Information Figure S2 for all individual data points). For *A. cylindrica*, heterocyst distance increased continuously with pN_2 and through culture growth phase. For *A. variabilis*, heterocyst distance did not appear to correlate with pN_2

intervals (Wald intervals) as detailed in Supporting Information Appendix S5. The resulting analytical precision (σ_a) estimated for the derived ${}^{15}\varepsilon_{Norg/N2.gas}$ values by standard error propagation is 0.12‰ (i.e., dominated by the error in the bulk organic nitrogen isotope measurement). As with all isotope measurements, the accuracy of the measured ${}^{15}\varepsilon$ values is limited by the uncertainty of the reference materials.

2.4 | Data analysis

All calculations, data processing, and visualizations were performed in R (R Core Team, 2017) and are available online (see Supporting Information Appendix S1 for details). Briefly, the mean and standard error (*SE*) of the mean for all heterocyst distances (n_{cbh}) and isotopic data (${}^{15}\varepsilon_{Norg/N2.gas}$) visualized in Figures 4 and 5 were estimated by bootstrap (Efron & Tibshirani, 1998) with 1,000 resamplings with replacement and are summarized in the Supporting Information Tables S1, S3, and S5. The standard errors of parameters derived from linear and nonlinear least squares regression models were likewise estimated by bootstrap, and all regression estimates in this manuscript are reported with ±1 *SE*. The errors of variables used in equations to calculate derived quantities were propagated by standard error propagation assuming independent variables. Statistical significance of heterocyst distances ($\Delta\bar{n}_{cbh}$) between the different experimental conditions was evaluated by pairwise comparisons using both the Student's *t* test statistic of the bootstrapped distribution differences and the nonparametric Wilcoxon–Mann–Whitney test statistic (see Supporting Information Appendix S2 and Supporting Information Tables S2 and S4) with significance levels determined based on *p*-value cutoffs. Both tests yielded identical significance levels. Only *p*-values <0.05 were considered statistically significant.

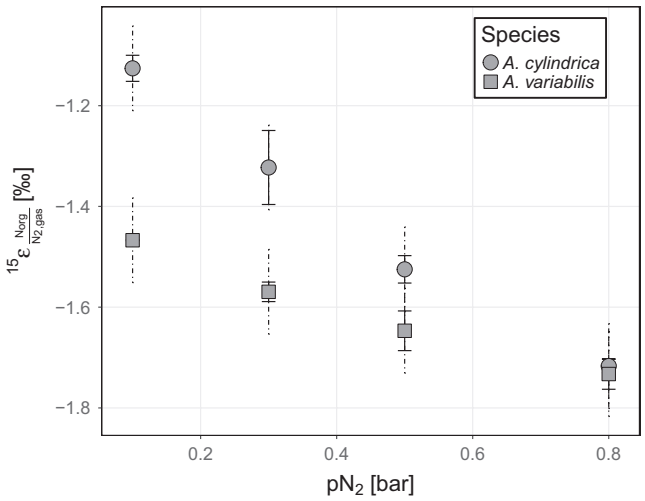

FIGURE 5 Nitrogen isotope fractionation in response to pN_2. *A. cylindrica* and *A. variabilis* cultures grown in the absence of fixed nitrogen under variable pN_2 were analyzed in stationary phase. Fractionation factors ($\varepsilon^{15}N_{Norg/N2.gas}$) are shown as the bootstrapped mean **(symbol)** and error of the mean (±1 *SE*; solid error bars) of all biological replicates (see Supporting Information Table S5 for data summary and Supporting Information Figure S8 for all data points). Dashed error bars show estimated analytical precision (σ_a). The overall fractionation factor ($\varepsilon^{15}N_{Norg/N2.gas}$) is correlated with pN_2 for both species, increasing in magnitude with pN_2

3 | RESULTS

Anabaena cylindrica and *Anabaena variabilis* cultures were grown under different nitrogen partial pressures without any added bioavailable fixed nitrogen. Partial pressures investigated were 0,

0.1, 0.3, 0.5, and 0.8 bar N_2. Growth in the absence of dinitrogen (pN_2 = 0 bar) was nonexistent (*A. cylindrica*) or minimal (*A. variabilis*) because the cultures were entirely dependent on nitrogen fixation as the sole available source of cellular nitrogen. Small amounts of growth in *A. variabilis* despite the absence of N_2 were likely a consequence of cellular nitrogen carryover from the inoculum. Maximal growth rates of both *A. cylindrica* and *A. variabilis* were significantly reduced at pN_2 < 0.5 bar (from $\mu = 0.89 \pm 0.12$ day^{-1} at 0.8 bar N_2 to 0.55 ± 0.12 day^{-1} at 0.1 bar N_2 for *A. cylindrica*, and from $\mu = 0.61 \pm 0.04$ day^{-1} at 0.8 bar N_2 to 0.45 ± 0.02 day^{-1} at 0.1 bar N_2 for *A. variabilis*) but showed no statistically significant growth inhibition at 0.5 bar and above (see Supporting Information Figures S5 and S6 for details). Similarly, Klinger, Mancinelli, and White (1989) observed reduced growth rates for *Azotobacter vinelandii* and *Azomonas agilis* at pN_2 < 0.4 bar, with a ~53% decrease in maximal growth rate from 0.8 to 0.1 bar N_2 for both species compared to a ~62% decrease for *A. cylindrica* and ~36% decrease for *A. variabilis*.

3.1 | Heterocyst spacing in response to N_2 partial pressure

Heterocysts in filaments grown under pN_2 > 0 bar were easily distinguishable from brighter vegetative cells because they showed reduced autofluorescence due to their lack of light-harvesting phycobiliprotein. A compilation of bright-field and fluorescence micrographs of *A. cylindrica* heterocystous filaments grown under each pN_2 condition (Figure 3) highlights the average increase in heterocyst distance observed at each increasingly higher pN_2 tested. Despite low or no growth at pN_2 = 0 bar, both species developed closely spaced heterocysts in the filaments of the inoculum but exhibited inconsistent and occasionally reversed patterns of autofluorescence that were not useful for heterocyst identification. These cultures likely succumbed to nitrogen starvation, so vegetative cells were unable to maintain phycobiliprotein and actively photosynthesize.

Heterocyst distances were quantified as the number of vegetative cells between heterocysts as described in Materials and Methods. The results are summarized as the bootstrapped mean and median heterocyst distances (Supporting Information Tables S1 and S3) for each culture growth phase tested and are visualized in Figure 4 (see Supporting Information Figure S2 for all data points). The heterocysts along *A. variabilis* filaments did not develop in a pattern that correlated with pN_2, but for *A. cylindrica* the average heterocyst distance increased by 2–3 cells for each subsequently higher pN_2 tested and as the culture progressed from early-exponential to stationary growth phase. The results show that heterocyst distances in *A. cylindrica* were significantly shorter in filaments cultivated at lower N_2 partial pressures than at higher pN_2 (p-value < 0.001 for all pairwise comparisons, Supporting Information Table S2), while only the pN_2 = 0 bar condition showed significantly shorter heterocyst distances for *A. variabilis* (Supporting Information Table S4).

3.2 | Nitrogen isotope fractionation in response to N_2 partial pressure

Biological samples from replicate heterocyst experiments were collected to evaluate whether the pN_2 is reflected isotopically in the biomass produced by nitrogen fixation in cultures of *Anabaena* sp. The observed fractionation factor between biomass nitrogen and headspace N_2 ($^{15}\varepsilon_{Norg/N2.gas}$) of each culture was determined (see summary in Supporting Information Table S5). Experiments at pN_2 = 0 bar did not yield enough biomass for isotopic measurements and were excluded from the analysis. Observed fractionation factors showed a clear trend with pN_2 for both species (Figure 5), and the pattern indicates that discrimination between ^{14}N and ^{15}N increased with pN_2, leading to more ^{15}N-depleted biomass at high pN_2. However, the change was more pronounced for *A. cylindrica* (from $\varepsilon^{15}N_{Norg/N2.gas}$ = −1.13‰ at 0.1 bar to −1.72‰ at 0.8 bar) than for *A. variabilis* (from $\varepsilon^{15}N_{Norg/N2.gas}$ = −1.47‰ at 0.1 bar to −1.73‰ at 0.8 bar) with both species showing the same fractionation at pN_2 = 0.8 bar. The $\varepsilon^{15}N$ of both species fell within the range of previously measured values for diazotrophic cyanobacteria grown under ~0.8 bar N_2 ($\varepsilon^{15}N_{Norg/N2.gas}$ = 0.5 to −2.8‰; Minagawa & Wada, 1986; Macko, Fogel, Hare, & Hoering, 1987; Bauersachs et al., 2009) and for *A. variabilis* grown in high Mo, Fe, and P concentrations similar to our media ($\varepsilon^{15}N_{Norg/N2.gas}$ = −1.4 to −1.93‰; Zerkle, Junium, Canfield, & House, 2008).

4 | DISCUSSION

4.1 | Heterocyst spacing in *Anabaena cylindrica*

Our findings support the hypothesis that heterocyst spacing is regulated by pN_2 in *Anabaena cylindrica*. Overall, the average distance between heterocysts increased with pN_2 (Figure 4), highlighting the possible role of enzyme kinetics under substrate limitation (the intercellular level of N_2) as a rate-limiting factor in interval lengthening. Implicit in the assumption that the heterocyst pattern is a direct, population-scale reflection of the changing kinetics of nitrogen fixation is that heterocysts must be the only site of nitrogen fixation in the filaments and that nitrogen fixation by individual heterocysts is limited only by the kinetics of the nitrogenase enzyme. Under these conditions, the total flux of fixed nitrogen available to the whole population for growth ($\phi_{fix.total}$) is dependent solely on the number of heterocysts (n_{het}) and the flux of fixed nitrogen from the individual heterocysts (ϕ_{fix}). This flux follows the constraints of Michaelis–Menten kinetics $\left(\phi_{fix} = V_{max} \cdot \frac{C_{N2.het}}{C_{N2.het+K_M}}\right)$ with a maximum rate of catalysis (V_{max}) and characteristic half-saturation constant (K_M) for the substrate ($C_{N2.het}$, the concentration of dissolved N_2 inside the heterocysts, which scales with pN_2 but is not identical to it). From this: $\phi_{fix.total} = n_{het} \cdot \phi_{fix} = n_{het} \cdot V_{max} \cdot \frac{C_{N2.het}}{C_{N2.het+K_M}}$. The rate of growth of the vegetative cells ($\mu \cdot n_{veg}$) must be balanced by this nitrogen supply rate from the heterocysts (with some yield proportionality K_Y) because nitrogen is the limiting nutrient in this experimental system. Thus, $\mu \cdot n_{veg} = K_Y \cdot n_{het} \cdot V_{max} \cdot \frac{C_{N2.het}}{C_{N2.het+K_M}}$. The ratio of vegetative to heterocyst

cells $\left(\frac{n_{veg}}{n_{het}}\right)$ represents the *number of vegetative cells between heterocysts* (n_{cbh}) measured in this study (Figure 4), which implies the following relationship:

$$n_{cbh} = \frac{K_Y}{\mu} \cdot \frac{V_{max} \cdot C_{N2.het}}{C_{N2.het} + K_M}. \quad (3)$$

This conceptualization of the heterocyst spacing as a direct reflection of the balance between filament growth and nitrogen supply rate is consistent with a model of one-dimensional distribution of, and heterocyst differentiation triggered by, fixed nitrogen along the filament. Flores, Herrero, Wolk, and Maldener (2006) suggest that the periplasm serves as a channel through which substances can be exchanged between heterocysts and vegetative cells. Given that this transport is extremely rapid (Wolk, Austin, Bortins, & Galonsky, 1974; Wolk, Thomas, & Shaffer, 1976) and thus likely mediated by passive diffusion, the rate at which fixed nitrogen propagates along the filament away from the heterocysts should be proportional to the rate of fixation. Assuming a steady consumption rate of fixed nitrogen by vegetative cells over the timescale of each generation, the distance a pool of organic nitrogen can emanate from heterocysts before being completely metabolized by the intervening vegetative cells will depend on its rate of synthesis. As a direct consequence of this balance between growth and nitrogen supply rate during filament lengthening, the vegetative cells midway between existing heterocysts would become starved of fixed nitrogen, thereby triggering their differentiation into heterocysts (Yoon & Golden, 2001). Indeed, NanoSIMS analyses coupled with ^{15}N-enriched isotope tracers show a midpoint depletion of fixed nitrogen between heterocysts (Popa et al., 2007). Interestingly, Popa et al. did not observe a gradient of nitrogen fixation products, as the rate of fixed nitrogen transport far exceeded its rate of consumption by vegetative cells. Heterocyst spacing would be most sensitive at low substrate concentration (i.e., low pN_2, where the enzyme kinetics of nitrogenase change the most in response to substrate variation) and would asymptotically approach a maximum value with increasing substrate concentration (i.e., high pN_2, where nitrogenase activity is at V_{max}), as observed for *A. cylindrica* (Figure 4). Assuming V_{max} remains constant (i.e., assuming that heterocysts cannot change the amount of nitrogenase in response to N_2 concentrations), the heterocyst spacing and growth rate data from *A. cylindrica* in exponential growth (conceptualized in Equation 3 and visualized in Figure 4 and Supporting Information Figure S6, respectively) can be combined with the isotopic data (Figure 5) to derive an estimate of the half-saturation constant K_M for nitrogenase from the measured heterocyst distances. K_M is divided by K_H, Henry's law solubility constant for N_2 in water (6.5×10^{-4} mol L^{-1} bar^{-1} at 25°C; Sander, 2015) to convert to pressure units. The resulting values of K_M/K_H for *A. cylindrica* are as follows: 0.120 ± 0.034 bar N_2 for early-exponential phase and 0.121 ± 0.014 bar N_2 for late-exponential phase. K_M for stationary phase could not be calculated because growth rate data were not obtained for this phase. For a more complete derivation of K_M and details on the model, see Supporting Information Appendix S5 and Supporting Information Appendix S6. Our purely heterocyst-based estimates of K_M are consistent with previous estimates of the half-saturation constants of nitrogenase in *Anabaena* sp. (ranging from 0.12 to 0.20 bar N_2; for more detailed comparison, see summary in Supporting Information Table S6).

The presented model of heterocyst spacing captures first-order aspects of the physiological response of *A. cylindrica*. However, the model likely oversimplifies the biophysical mechanisms occurring. The significant variation in spacing observed between individual filaments (Supporting Information Figure S2) and across cultures grown under the same pN_2 but measured at different growth stages (Figure 4 and Supporting Information Figure S3) highlights the important influence of additional factors on heterocyst spacing. Developmental controls undeniably play an important role in heterocyst development through the expression of regulatory genes that promote differentiation, such as *ntcA* and *hetR* (Buikema & Haselkorn, 1991; Wei, Ramasubramanian, & Golden, 1994), as well as the synthesis of inhibitory molecules that prevent differentiation, such as PatS and HetN (Callahan & Buikema, 2001; Yoon & Golden, 2001). Furthermore, several studies (Adams & Carr, 1989; Brown & Rutenberg, 2014; Meeks & Elhai, 2002) have suggested that heterocyst differentiation may be influenced by cell cycle timing, so it is possible that the variation in heterocyst spacing observed within identical pN_2 cultures is a consequence of filament cell cycles. Though this phenomenon was not investigated at the individual cellular level here, the slight differences in heterocyst spacing between growth stages highlight the possible macroinfluence of culture growth phase on heterocyst differentiation. Within each pN_2 condition tested for *A. cylindrica*, the average heterocyst distance increased as the cultures progressed through the early-exponential, late-exponential, and death phases (Supporting Information Figure S3), potentially as a consequence of the increasing energy and nutrient deprivation. Vegetative cells are energetically inexpensive, but heterocysts present a substantial energy burden to the filaments, as they are terminally differentiated so do not divide to yield carbon-fixing cells. The exponential phase of culture growth is characterized by rapid cell division, which likely includes rapid heterocyst differentiation. During this phase, shorter heterocyst intervals were possibly maintained because the abundance of media nutrients enabled heterocyst differentiation to keep up with vegetative cell division. Upon nutrient depletion (late-exponential phase), the rate of vegetative cell division may have surpassed differentiation of heterocysts, causing an overall lengthening of heterocyst intervals. Heterocyst differentiation may have completely halted in the culture death phase, but resilient vegetative cells continuing to divide with residually available fixed nitrogen would have furthered filament lengthening. Additionally, vegetative cells may have consumed fixed nitrogen at higher rates during the early stages of culture growth, which could have also led to the shorter intervals observed.

N_2 partial pressure was the only changed parameter across all samples in this study, suggesting a strong link between pN_2 and the physiological response observed despite the existence of other experimental variables. Indeed, cultures grown in nitrate-rich

medium under different pN_2 show nearly identical growth patterns (Supporting Information Figure S4), while pN_2 distinctly affects culture growth under nitrogen-fixing conditions (Supporting Information Figure S5). Such results highlight the real, observed influence of pN_2 on *Anabaena* cellular physiology. Though an invariable atmosphere achieved through a pH-stated continuous-flow culture would have been ideal, such a setup was beyond the scope of this initial study. Instead, O_2 buildup, inorganic carbon depletion, and pH variation in the media were minimized by daily headspace flushing, and cultures were agitated constantly to ensure continuous nutrient mixing, facilitate gas equilibration, and prevent localized O_2 buildup and CO_2/N_2 depletion. Indeed, O_2 did not rise above atmospheric levels in any sample, thereby maintaining conditions necessary for optimum nitrogenase activity (Stewart & Pearson, 1970). Though these variables may have affected the nitrogen fixation dynamics, such changes were observed across all pN_2 conditions and thus affected nitrogenase activity similarly.

Overall, we conclude that the heterocyst pattern in *A. cylindrica* is clearly and systematically influenced by pN_2, but the extent to which this is physiologically regulated, and the direct mechanisms underlying this response merit further investigation.

4.2 | Heterocyst spacing in *Anabaena variabilis*

Heterocysts must be the only site of nitrogen fixation in the cyanobacterial population in order for the derived enzyme kinetics-driven interpretation to be applied to heterocyst spacing. As expected, this does *not* appear to be the case for *A. variabilis*. The fact that pN_2 failed to engender significant change in the heterocyst pattern along *A. variabilis* filaments likely reflects the expression of nitrogenase in the vegetative cells (Nif2) and heterocysts (Nif1). Our experimental setup was anaerobic (CO_2/N_2/He only), thus promoting expression of both *nif1* and *nif2* from the start; however, any buildup of molecular oxygen produced by the photosynthetic vegetative cells between daily headspace sparging may have temporarily suppressed *nif2* expression within the vegetative cells. This inconsistent expression, coupled with the lack of a solely heterocyst-dependent transport of organic nitrogen along the filaments, likely led to the development of a random heterocyst pattern for *A. variabilis* (Figure 4).

Our model for heterocyst spacing assumes that intracellular nitrogen starvation triggers heterocyst differentiation. Therefore, it is perhaps puzzling why both Nif1 and Nif2 nitrogenases simultaneously operate and heterocysts develop in *A. variabilis* despite the fact that individual vegetative cells should not be nitrogen-starved because Nif2 can fully support the nitrogen needs of the filaments (Thiel et al., 1995). To explain this fact, as well as observations that heterocysts can still differentiate in mutant *Anabaena* organisms incapable of nitrogen fixation by Nif1 nitrogenase (Buikema & Haselkorn, 1991; Thiel & Leone, 1986; Wilcox, Mitchison, & Smith, 1975), Thiel and Pratte (2001) propose that heterocyst development is not controlled by the nitrogen insufficiency of individual cells and furthermore that the heterocyst spacing pattern is not influenced by products of nitrogen fixation. However, results from our *A. cylindrica* experiments (Figure 4) clearly demonstrate that a nitrogenase-controlled transport of organic nitrogen influences the spaced pattern of heterocysts, suggesting a prominent role of nitrogen starvation as a trigger for differentiation. Furthermore, the mutants studied by Thiel and Leone and Wilcox et al. were generated by mutagenesis techniques, which likely disrupted other nontargeted genes involved in heterocyst differentiation (see table 1 in Herrero, Muro-Pastor, Valladares, & Flores, 2004 for comprehensive list of known genes) in addition to those that encode nitrogenase and thus do not provide reliable information regarding controls on heterocyst development. Additionally, Wilcox et al. (1975) exclusively examined the initial heterocyst pattern, as the *A. cylindrica* mutants could not continue to grow without bioavailable nitrogen. Differences likely exist between the mechanisms that establish the heterocyst spacing in response to initial nitrogen deprivation and those that maintain the spacing thereafter. It is clear that the efficiency of nitrogen production by nitrogenase in heterocysts significantly affects the overall regulatory mechanism for heterocyst differentiation (after the initial spacing pattern has formed), but it is likely not the only regulator. In fact, the results obtained by Buikema and Haselkorn (1991)—that *Anabaena* 7120 mutants carrying an extra copy of *hetR* develop heterocysts despite lacking nitrogen fixation capabilities—highlight one particular genetic control on heterocyst development. Likewise, for *A. variabilis*, developmental factors probably contribute to redundant expression of Nif1 and Nif2 nitrogenases during external nitrogen deficiency, as extra fixed nitrogen may increase the organisms' chances of survival (Thiel & Pratte, 2001). Though it is clear that the heterocyst pattern is at least partially controlled by nitrogenase kinetics, it is unclear whether this influence is direct (via the rate of fixed nitrogen distribution) or indirect (via effects on expression of heterocyst-related genes such as *hetR* and *patS*). Future studies should elucidate how this effect is mediated.

4.3 | Heterocyst spacing as paleoproxy for atmospheric N_2 levels

This study reinforces the notion that morphological features in preserved cyanobacteria filaments may be useful to understand ancient atmospheric N_2 levels. However, the lack of reliable fossil heterocysts in the Precambrian record poses a significant challenge to the application of this paleobarometer. Fossilized cyanobacteria with convincing heterocysts have been found in the 400-million-year (Ma)-old Rhynie Chert of Scotland (Croft & George, 1959), but most reports of older fossil heterocysts (e.g., Figure 6; Schopf, 1968; Licari & Cloud, 1968, 1972; Cloud, 1976; Awramik & Barghoorn, 1977; Nagy, 1978) are disputed, so cannot reliably be used for interpreting ancient pN_2. Heterocysts may be absent from the early geologic record because they were not well preserved during Earth's history or have been largely overlooked thus far (Golubic, Sergeev, & Knoll, 1995; Pang et al., 2018). Alternatively, heterocystous cyanobacteria may have evolved well after other cyanobacterial assemblages, as has been proposed following phylogenetic analyses of single genes (e.g., 16S rRNA; Giovannoni et al., 1988; Turner, Pryer, Miao,

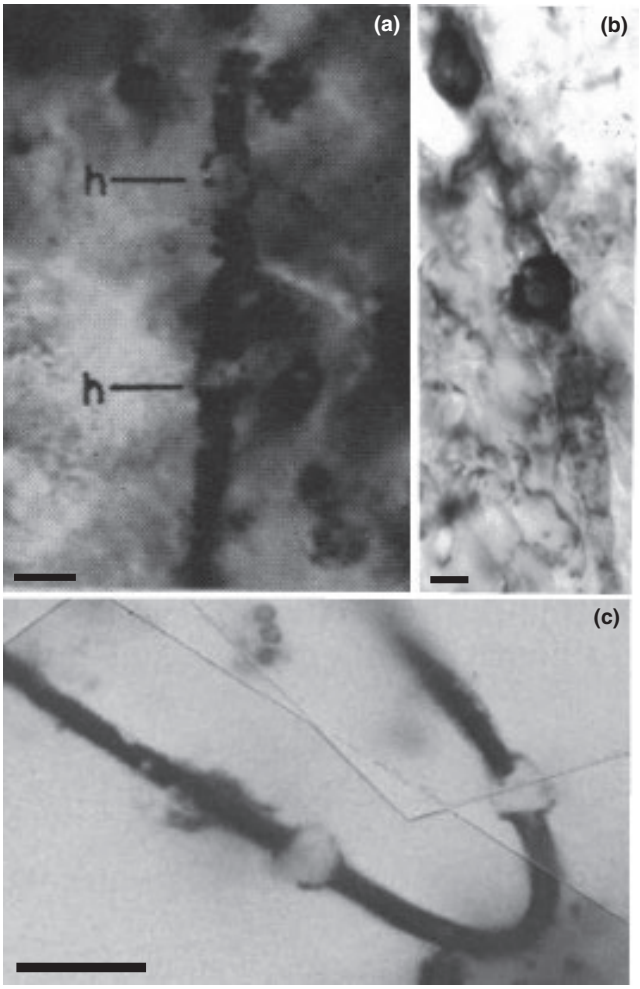

FIGURE 6 Fossilized cyanobacteria filaments with two purported yet presently disputed heterocysts. Shown are fossils from (a and c) ~2 Ga old Gunflint Iron Formation, southern Ontario (Awramik & Barghoorn, 1977; Licari & Cloud, 1968); and (b) ~2.3 Ga old Malmani Dolomite, South Africa (Nagy, 1978). Scale bar = 5 μm in all figures

& Palmer, 1999) and of multiple genes combined with morphological characters (Sanchez-Baracaldo, Hayes, & Blank, 2005). Due to the nonuniform rates of gene mutation across species, these techniques cannot accurately date the evolution of this cyanobacterial clade. However, heterocystous cyanobacteria likely arose after atmospheric O_2 reached concentrations high enough to inhibit nitrogenase (Olson, Reinhard, & Lyons, 2016; Tomitani, Knoll, Cavanaugh, & Ohno, 2006)—that is, during the Proterozoic eon (Berman-Frank, Chen, Gerchman, Dismukes, & Falkowski, 2005; Holland & Beukes, 1990), although oxygenic "whiffs" may have appeared in the Archean (Anbar et al., 2007). Time calibrations based on integrated phylogenetic and phenotypic data suggest that heterocystous cyanobacteria evolved 2,450–2,100 Ma ago (Tomitani et al., 2006), but possibly more recently (Uyeda, Harmon, & Blank, 2016). The presence of akinetes in the fossil record may additionally provide a minimum age constraint for the evolution of heterocysts, as akinetes are exclusively a feature of heterocystous cyanobacteria today (Castenholz, 2001) and likely arose after heterocysts (Sanchez-Baracaldo et al., 2005). Akinete fossils have been discovered in cherts ranging from 2,000 to 720 Ma old (Amard & Bertrand-Sarfati, 1997; Golubic et al., 1995; Pang et al., 2018; Sergeev, 2009; Sharma, 2006; Srivastava, 2005; Tomitani et al., 2006). In addition to the need for more reliable heterocystous fossils, further work is necessary to conclusively ascertain that heterocyst spacing in fossils such as these will be useful as a paleobarometer.

The relationship between heterocyst distance and pN_2 is not without ambiguity. The wide distribution of interval lengths observed at each pN_2 challenges the ability to extrapolate information about ancient pN_2 unless a statistically significant number of samples can be collected from rocks. Although statistical analyses of the correlation between heterocyst intervals along each filament were not performed, such correlation is likely given the clonal nature of the cells during filament lengthening. A nonzero covariance would reduce the statistical significance of the mean heterocyst distance as a function of pN_2. Future work must examine this relationship to inform how many fossil filaments are necessary to measure pN_2 with statistical confidence. With current microscopy techniques that involve thin sectioning of rock samples, filaments must be oriented parallel to the thin section in order to be preserved during sample preparation, which increases the difficulty of finding intact filaments. However, new 3D microscopy techniques (e.g., high-resolution neutron imaging; Jakubek, Pospisil, Vacik, & Vavrik, 2012) that do not require thin sectioning of rock samples may enable heterocystous filaments to be found in larger volumes than permitted by thin sections, which could help circumvent existing challenges of finding fossilized cyanobacteria. Despite likely future improvements in microscopy techniques, any potentially quantifiable relationship is further complicated by the fact that heterocyst spacing does not remain constant throughout culture growth. In addition, the effect of pN_2 on heterocyst spacing appears to be limited to particular organisms, as *A. variabilis* did not respond to pN_2 in the same manner as *A. cylindrica*. Thus, differentiating between species in the rock record would be necessary but challenging. Finally, this physiological response must be interrogated in natural cyanobacterial communities that have the propensity to become preserved in the fossil record. In dense cyanobacterial blooms where the dissolved O_2 concentration and pH can become very high, while inorganic carbon and nutrients can become very low, filament physiology and nitrogenase activity may be significantly affected compared to responses observed in a laboratory setting.

4.4 | Nitrogen isotope fractionation in *Anabaena* species

We observed a strong correlation between pN_2 and the nitrogen isotope fractionation ($\varepsilon^{15}N_{Norg/N2.gas}$) of *Anabaena cylindrica* and *Anabaena variabilis* filaments. Under the modern atmosphere of 0.8 bar N_2, nitrogenase tends to discriminate against ^{15}N by up to 2.8‰ (Bauersachs et al., 2009; Macko et al., 1987; Minagawa & Wada, 1986). Here, we show that low N_2 availability creates a

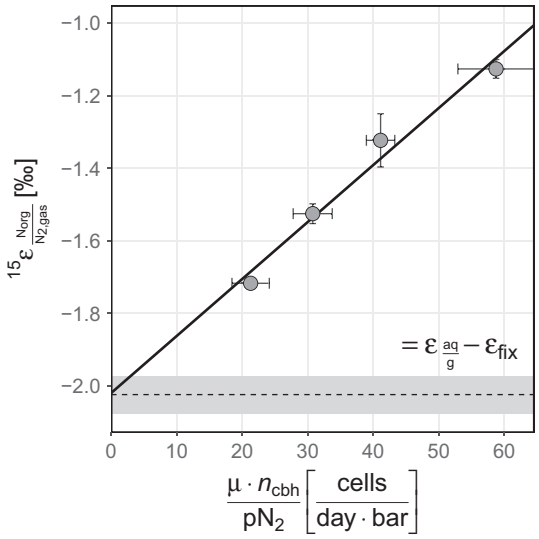

FIGURE 7 N_2 partial pressure (pN_2), growth rate (μ), and heterocyst spacing (n_{cbh})-dependent isotope model. The intercept provides the first in vivo estimate of the intrinsic isotope fractionation factor of nitrogenase (ε_{fix} = −2.71 ± 0.090; bootstrap estimate ±1 *SE*) and is based on data from *A. cylindrica* cultures grown under variable pN_2. Horizontal dashed line indicates the bootstrapped regression estimate of $\varepsilon_{aq/g} - \varepsilon_{fix}$ (−2.02 ± 0.050 based on literature data on $\varepsilon_{aq/g}$—see Supporting Information Figure S11)

reservoir effect within the cells—that is, the intracellular and extracellular N_2 pools are *not* exchanged rapidly enough, relative to N_2 consumption by nitrogenase, to ensure complete isotopic equilibration of N_2 (and thus maximal expression of the isotope effect of nitrogenase). In contrast, high N_2 availability increases the exchange of N_2 into and out of the cells, leading to faster isotopic equilibration of N_2 and enabling the intrinsic isotopic fractionation of nitrogenase (ε_{fix}, see Supporting Information Figure S10) to be maximally expressed.

The overall fractionation by *A. variabilis* is more pronounced at lower pN_2 than the fractionation by *A. cylindrica* (Figure 5) because nitrogenase in *A. variabilis* is expressed in the vegetative cells *and* in the heterocysts. With nitrogen fixation distributed among both types of cells, each individual cell is less diffusion limited, leading to a smaller reservoir effect. In contrast, nitrogenase is localized to the heterocysts in *A. cylindrica*, rendering each nitrogen-fixing cell responsible for a larger burden of fixation and imposing greater N_2 diffusion limitations along its filaments. These physiological effects likely contributed to the different isotope signatures of fixation observed at each pN_2 condition. Contribution to this fractionation by alternative nitrogenases, which have been shown to express different fractionation factors in vivo (Rowell, James, Smith, Handley, & Scrimgeour, 1998; Zhang et al., 2014), can be ruled out because *A. cylindrica* only possesses a single Mo-nitrogenase (Attridge & Rowell, 1997) and *A. variabilis* was not starved of molybdenum (see Materials and Methods), which would have otherwise triggered synthesis of the vanadium-dependent nitrogenase (Thiel, 1993). Importantly, this speculative link between the isotopic effect and heterocyst number is merely a hypothesis suggested by our observed data and should be further investigated. Previous studies have shown that heterocyst frequency does not directly correlate with nitrogenase activity (e.g., Kangatharalingam, Priscu, & Paerl, 1992), and we acknowledge this relationship is likely more complex than our interpretation. However, given that pN_2 exerts a clear influence on heterocyst frequency (Figure 4), we interrogate our data under the assumption that (with all other parameters equal) pN_2 affects the kinetics of nitrogenase.

The observed reservoir effects are analogous to similar phenomena observed for various carbon fixation systems (Farquhar, 1982; Laws, Popp, Bidigare, Kennicutt, & Macko, 1995). Such systems have been well described by metabolic flux models relating the observed isotope fractionation to the intrinsic isotope effects of the individual reaction steps, their relative reversabilities, and the concentrations of the relevant substrates (Farquhar, 1982; Guy, Reid, & Krouse, 1986; Hayes, 2001; Laws et al., 1995). Following the approach employed by Laws et al. (1995) to understand the growth rate-dependent organismal isotope effect during carbon fixation in phytoplankton, we derive a steady-state model (see Supporting Information Appendix S5 and Supporting Information Figure S10 for details) that relates the observed organismal isotope fractionation ($\varepsilon_{Norg/N2.gas}$) to the partial pressure of N_2 (pN_2), the growth rate (μ), and the heterocyst spacing (n_{cbh}):

$$\varepsilon_{\frac{Norg}{N2.gas}} = \varepsilon_{\frac{aq}{g}} - \varepsilon_{fix} + \frac{\varepsilon_{fix}}{K_1 \cdot K_Y \cdot K_H} \cdot \frac{\mu \cdot n_{cbh}}{pN_2}, \quad (4)$$

where $\varepsilon_{aq/g}$ is the equilibrium fractionation factor between the aqueous and gaseous phase of N_2; ε_{fix} is the intrinsic kinetic isotope fractionation factor of nitrogenase during the nitrogen fixation; and K_1, K_Y, and K_H are the N_2 diffusion rate constant, growth yield, and Henry's constant, respectively. In combination with available experimental literature data on $\varepsilon_{aq/g}$ (Supporting Information Figure S11; Klots & Benson, 1963; Knox, Quay, & Wilbur, 1992; Lee, Sharp, & Fischer, 2015), Equation 4 enables an in vivo estimate of the intrinsic isotope fractionation factor of nitrogenase (ε_{fix}) from the intercept of the regression of $\varepsilon_{Norg/N2.gas}$ versus $\frac{\mu \cdot n_{cbh}}{pN2}$ as illustrated in Figure 7 (with $\varepsilon_{aq/g}$ = 0.70 ± 0.080). Because this derivation requires that nitrogen fixation occurs exclusively in heterocysts in the cyanobacterial population, only data from *A. cylindrica* are used to estimate ε_{fix}. The additional proportionality constants K_1 and K_Y included in the slope of the regression cannot be fully resolved in this study but may be of interest in future work.

Our study is the first in vivo estimate of the intrinsic isotope effect of nitrogenase itself (ε_{fix} = −2.71 ± 0.09‰) for the overall isotope fractionation in nitrogen fixation ($\varepsilon_{Norg/N2.gas}$). To our knowledge, the only other available estimate is based on in vitro work with purified nitrogenase extracts (Sra et al., 2004) that yielded a significantly larger ε_{fix} (in excess of 10‰). This discrepancy possibly arose from our examination of this isotope effect

in *A. cylindrica* versus *Azotobacter vinelandii* by Sra et al. (2004). Though both species express Mo-nitrogenase, *A. cylindrica* and *A. vinelandii* are distantly related (Boyd & Peters, 2013), so their nitrogenases may be genetically different enough to produce distinct intrinsic isotope effects. Different values obtained for the ε_{fix} of nitrogenase may also reflect major experimental differences between the in vivo and in vitro experiments. The pH, O_2, and inorganic carbon variation (discussed in Section 4.1) may have also affected nitrogenase activity in this study. Although this discrepancy cannot be resolved at present, our study opens the door for future possibilities of measuring the currently unknown intrinsic ε_{fix} of other nitrogenases and highlights the merits of combined work with purified nitrogenases and environmentally controlled studies at varying pN_2 and/or growth rates.

4.5 | Nitrogen isotope fractionation as a paleoproxy for atmospheric N_2 levels

The distinct effect of pN_2 on the isotope fractionation of nitrogen imparted by nitrogenase strongly points to biological $\delta^{15}N$ as a paleoproxy for pN_2. In contrast to heterocyst spacing, biological $\delta^{15}N$ signatures (reported in this study as $\varepsilon^{15}N$) can be expected in the Archean given that nitrogen fixation is an ancient metabolism (Boyd & Peters, 2013; Fani et al., 2000; Stüeken et al., 2015). The nitrogen isotope record spans most of Earth's history and has been widely interrogated (e.g., Beaumont & Robert, 1999; Stüeken, Kipp, Koehler, & Buick, 2016), yet the direct influence of pN_2 on $\delta^{15}N$ of ancient biomass produced by nitrogenase has not yet been explored. Interpreting nitrogen isotope data from this perspective could lead to insight into the paleoatmospheric pressure and composition, as well as a greater understanding of ancient global nitrogen biogeochemical cycles.

Stüeken, Kipp, Koehler and Buick (2016) provide a comprehensive review of the nitrogen isotope record to investigate how Earth's nitrogen cycle has evolved through the major eras. Briefly, while the Paleoarchean record is poorly preserved and has yet to offer compelling information about its nitrogen cycle, average $\delta^{15}N$ values of the Mesoarchean (+1.1 ± 1.9‰) support the role of nitrogen fixation as the dominant microbially mediated process. Importantly, Mo-nitrogenase may have evolved by 3.2 Ga (Stüeken et al., 2015), and Mo appears to have been sufficiently available to support its metabolism at this time (Glass, Simon-Wolfe, Elser, & Anbar, 2010; Planavsky et al., 2014; Zerkle, House, Cox, & Canfield, 2006). Between the Mesoarchean and late Paleoproterozoic, average $\delta^{15}N$ values become progressively heavier (generally up to ~+10‰), reflecting the emergence of an aerobic nitrogen cycle and increasingly enhanced rates of denitrification (Garvin, Buick, Anbar, Arnold, & Kaufman, 2009; Stüeken, Kipp, Koehler, & Buick, 2016). The Mesoproterozoic is characterized by localized euxinic, oxic, and anoxic regions of the ocean (Anbar & Knoll, 2002; Planavsky et al., 2011; Shen, Knoll, & Walter, 2003). Isotopic evidence supports the hypothesis that, during this time, nitrification and denitrification prevailed in surface and coastal waters ($\delta^{15}N$ up to +5‰), while nitrogen fixation dominated in the deep ocean ($\delta^{15}N$ = −2 to +2‰; Stüeken, 2013). From the late Neoproterozoic onwards, the nitrogen cycle has resembled that of the modern ocean (Ader et al., 2014).

In addition to the evolving redox states of Earth's ocean, $\delta^{15}N$ trends through history could reflect higher atmospheric pN_2 and/or lower biomass of diazotrophs in the past (Figure 7). More specific conclusions about ancient pN_2 cannot presently be drawn using our data due to several limitations of both the $\delta^{15}N$ record and our paleoproxy. Most importantly, more $\delta^{15}N$ measurements from Precambrian rocks are needed, yet the geologic record of early Earth is not well preserved due to metamorphic and diagenetic overprints that obscure $\delta^{15}N$ signals (Stüeken, Kipp, Koehler, & Buick, 2016). Denitrification can also mask the isotope effect of nitrogen fixation (Sigman & Casciotti, 2001), so our paleoproxy may be best applied to ancient fixed nitrogen that did not undergo subsequent alteration. Biological nitrogen preserved from the early Archean may satisfy such conditions, as nitrogen fixation dominated while denitrification was virtually nonexistent during this time (Stüeken et al., 2015; Thomazo & Papineau, 2013). However, given that heterocystous cyanobacteria likely evolved well after the early Archean (Tomitani et al., 2006; Uyeda et al., 2016), information on the pN_2-dependent isotopic response of nonheterocystous diazotrophs is needed to more reliably interrogate $\delta^{15}N$ from early Earth through this approach. For example, *Chroococcidiopsis thermalis* PCC 7203 (Thiel & Pratte, 2014) and *Trichodesmium* IMS101 (Dominic, Zani, Chen, Mellon, & Zehr, 2000) express nitrogenases that are genetically similar to Nif2 of *A. variabilis*. Additional places in the geologic record where $\delta^{15}N$ may exclusively reflect nitrogen fixation are sediments preserved from regions of the ocean that experienced euxinia, as such conditions inhibit nitrification and denitrification (Ward, 2008). However, because euxinia can reduce the bioavailability of Mo (Helz et al., 1996), conditions in these regions may have been more favorable to alternative nitrogenases than to Mo-nitrogenase (Zhang et al., 2014). Thus, our $\delta^{15}N$ paleoproxy would benefit from added insight into the effect of pN_2 on the isotope fractionation by alternative nitrogenases. Finally, the relatively small influence of pN_2 on the isotope variation observed in this study necessitates greater analytical precision of $\delta^{15}N$ measurements in rocks than is currently available.

5 | CONCLUSION

Cyanobacteria are an ancient lineage of organisms that continue to thrive today. As such, current species can be used as proxies for ancestral strains, enabling extrapolation about their environmental conditions. We have shown that *Anabaena cylindrica* record pN_2 levels in heterocyst formation patterns, while *Anabaena variabilis* filaments do not express a heterocyst pattern in response to pN_2. This response may therefore be species-specific. Furthermore, the large biological variability in heterocyst spacing observed at each pN_2 condition challenges the use of this morphological phenomenon

as a geobarometer because of necessary statistical requirements. Heterocyst spacing of cyanobacteria with Nif1 nitrogenase may instead be used to infer biochemical parameters about nitrogen fixation, such as K_M.

We have further shown that pN_2 can be recorded in the nitrogen isotope composition of both *A. cylindrica* and *A. variabilis* filaments. The wide range of $\delta^{15}N$ measurements from ancient sediments has motivated extensive research seeking to understand ancient oceanic and atmospheric conditions that led to these values, but to our knowledge, no interpretation of cyanobacteria-relevant $\delta^{15}N$ signatures has taken pN_2 into consideration. Thus, if biomass from nitrogen-fixing bacteria is preserved in the rock record, applying our isotope data to cyanobacteria-specific, unaltered $\delta^{15}N$ measurements may lead to the development of a new paleobarometer for N_2.

Future work should further investigate the relationship between pN_2, heterocyst distance, and nitrogen isotopic effect; interrogate these responses at high pN_2 (>0.8 bar); and refine the limitations of their use as paleoproxies. Application of these tools to the geologic record will ultimately contribute to a better understanding of the ancient atmosphere and past nitrogen biogeochemical cycles.

ACKNOWLEDGMENTS

We thank Brett Davidheiser-Kroll and the University of Colorado Earth Systems Stable Isotopes Lab (CUBES-SIL), as well as Angela Detweiler and the Microbial Ecology/Biogeochemistry Lab at NASA Ames, for instrumentation that benefitted this project. We also thank members of the Kopf, Wing, Templeton, and Sepúlveda laboratories at CU Boulder, and the Bebout laboratory at NASA Ames, for helpful discussions, as well as the anonymous reviewers for constructive criticism that improved the manuscript. R. N. Gordon acknowledges James C. G. Walker for initial discussions on heterocyst spacing as a proxy for pN_2. S. M. Som and R. N. Gordon further discussed biobarometry at the "Re-conceptualizing the Origin of Life" Workshop held in Washington D.C. This work was supported in part by a NASA Exobiology grant (#80NSSC17K0667) and start-up funds from CU Boulder to S.H. Kopf, a Biological Sciences Initiative (BSI) Scholars grant from CU Boulder to S. N. Silverman, and a Science Innovation Fund (SIF) from NASA Ames to S. M. Som and B. M. Bebout. The Blue Marble Space Institute of Science Young Scientist Program administered the research experience of S. N. Silverman at NASA Ames. This paper is an outcome of the honors thesis of S. N. Silverman at CU Boulder.

ORCID

Shaelyn N. Silverman http://orcid.org/0000-0001-9201-6904
Sebastian H. Kopf http://orcid.org/0000-0002-2044-0201
Richard Gordon http://orcid.org/0000-0003-4970-9953
Sanjoy M. Som http://orcid.org/0000-0001-7684-0151

REFERENCES

Adams, D. G., & Carr, N. G. (1989). Control of heterocyst development in the cyanobacterium *Anabaena cylindrica*. *Journal of General Microbiology*, *135*, 839–849.

Ader, M., Sansjofre, P., Halverson, G. P., Busigny, V., Trindade, R. I. F., Kunzmann, M., & Nogueira, A. C. R. (2014). Ocean redox structure across the Late Neoproterozoic oxygenation event: A nitrogen isotope perspective. *Earth and Planetary Science Letters*, *396*, 1–13. https://doi.org/10.1016/j.epsl.2014.03.042

Amard, B., & Bertrand-Sarfati, J. (1997). Microfossils in 2000 Ma old cherty stromatolites of the Franceville Group, Gabon. *Precambrian Research*, *81*, 197–221. https://doi.org/10.1016/S0301-9268(96)00035-6

Anbar, A. D., Duan, Y., Lyons, T. W., Arnold, G. L., Kendall, B., Creaser, R. A., … Buick, R. (2007). A whiff of oxygen before the Great Oxidation Event? *Science*, *317*, 1903–1906. https://doi.org/10.1126/science.1140325

Anbar, A. D., & Knoll, A. H. (2002). Proterozoic ocean chemistry and evolution: A bioinorganic bridge? *Science*, *297*, 1137–1142. https://doi.org/10.1126/science.1069651

Attridge, E. M., & Rowell, P. (1997). Growth, heterocyst differentiation and nitrogenase activity in the cyanobacteria *Anabaena variabilis* and *Anabaena cylindrica* in response to molybdenum and vanadium. *New Phytologist*, *135*, 517–526. https://doi.org/10.1046/j.1469-8137.1997.00666.x

Avice, G., Marty, B., Burgess, R., Hofmann, A., Philippot, P., Zahnle, K., & Zakharov, D. (2018). Evolution of atmospheric xenon and other noble gases inferred from Archean to Paleoproterozoic rocks. *Geochimica et Cosmochimica Acta*, *232*, 82–100. https://doi.org/10.1016/j.gca.2018.04.018

Awramik, S. M., & Barghoorn, E. S. (1977). The Gunflint microbiota. *Precambrian Research*, *5*, 121–142. https://doi.org/10.1016/0301-9268(77)90025-0

Barry, P. H., & Hilton, D. R. (2016). Release of subducted sedimentary nitrogen throughout Earth's mantle. *Geochemical Perspectives Letters*, *2*, 148–159. https://doi.org/10.7185/geochemlet.1615

Bauersachs, T., Schouten, S., Compaoré, J., Wollenzien, U., Stal, L. J., & Damsté, J. S. S. (2009). Nitrogen isotopic fractionation associated with growth on dinitrogen gas and nitrate by cyanobacteria. *Limnology and Oceanography*, *54*, 1403–1411. https://doi.org/10.4319/lo.2009.54.4.1403

Beaumont, V., & Robert, F. (1999). Nitrogen isotope ratios of kerogens in Precambrian cherts: A record of the evolution of atmosphere chemistry? *Precambrian Research*, *96*, 63–82. https://doi.org/10.1016/S0301-9268(99)00005-4

Berman-Frank, I., Chen, Y.-B., Gerchman, Y., Dismukes, G., & Falkowski, P. (2005). Inhibition of nitrogenase by oxygen in marine cyanobacteria controls the global nitrogen and oxygen cycles. *Biogeosciences Discussion*, *2*, 261–273. https://doi.org/10.5194/bgd-2-261-2005

Berner, R. A. (2006). Geological nitrogen cycle and atmospheric N_2 over Phanerozoic time. *Geology*, *34*, 413–415. https://doi.org/10.1130/G22470.1

Boyd, E. S., & Peters, J. W. (2013). New insights into the evolutionary history of biological nitrogen fixation. *Frontiers in Microbiology*, *4*, 1–12.

Broda, E., & Peschek, G. A. (1983). Nitrogen fixation as evidence for the reducing nature of the early biosphere. *Biosystems*, *16*, 1–8. https://doi.org/10.1016/0303-2647(83)90021-7

Brown, A. I., & Rutenberg, A. D. (2014). A storage-based model of heterocyst commitment and patterning in cyanobacteria. *Physics Biology*, *11*, 016001.

Buick, R. (2008). When did oxygenic photosynthesis evolve? *Philosophical Transactions of the Royal Society B: Biological Sciences*, *363*, 2731–2743. https://doi.org/10.1098/rstb.2008.0041

Buikema, W. J., & Haselkorn, R. (1991). Characterization of a gene controlling heterocyst differentiation in the cyanobacterium *Anabaena*

7120. *Genes & Development*, *5*, 321–330. https://doi.org/10.1101/gad.5.2.321

Busigny, V., Cartigny, P., & Philippot, P. (2011). Nitrogen isotopes in ophiolitic metagabbros: A re-evaluation of modern nitrogen fluxes in subduction zones and implication for the early Earth atmosphere. *Geochimica et Cosmochimica Acta*, *75*, 7502–7521. https://doi.org/10.1016/j.gca.2011.09.049

Callahan, S. M., & Buikema, W. J. (2001). The role of HetN in maintenance of the heterocyst pattern in *Anabaena* sp. PCC 7120. *Molecular Microbiology*, *40*, 941–950. https://doi.org/10.1046/j.1365-2958.2001.02437.x

Castenholz, R. W. (2001). The Archaea and the deeply branching and phototrophic bacteria. In D. R. Boone, & R. W. Castenholz (Eds.), *Bergey's manual of systematic bacteriology* (vol. 1, 2nd ed., pp. 474–487). New York , NY: Springer. https://doi.org/10.1007/978-0-387-21609-6

Cloud, P. (1976). Beginnings of biospheric evolution and their biogeochemical consequences. *Paleobiology*, *2*, 351–387. https://doi.org/10.1017/S009483730000498X

Croft, W. N., & George, E. A. (1959). *Blue-green algae from the Middle Devonian of Rhynie, Aberdeenshire*. Vol. 3. Bulletin of the British Museum (Natural History), Geology.

Dalton, H., & Postgate, J. (1969). Effect of oxygen on growth of *Azotobacter chroococcum* in batch and continuous cultures. *Journal of General Microbiology*, *54*, 463–473.

Dominic, B., Zani, S., Chen, Y.-B., Mellon, M. T., & Zehr, J. P. (2000). Organization of the *nif* genes of the nonheterocystous cyanobacterium *Trichodesmium* sp. IMS101. *Journal of Phycology*, *36*, 693–701. https://doi.org/10.1046/j.1529-8817.2000.99208.x

Efron, B., & Tibshirani, R. J. (1998). *An introduction to the bootstrap* (1st ed.). Boca Raton, FL: CRC Press LLC.

Eickmann, B., Hofmann, A., Wille, M., Hao Bui, T., Wing, B. A., & Schoenberg, R. (2018). Isotopic evidence for oxygenated Mesoarchaean shallow oceans. *Nature Geoscience*, *11*, 133–138. https://doi.org/10.1038/s41561-017-0036-x

Fani, R., Gallo, R., & Lio, P. (2000). Molecular evolution of nitrogen fixation: The evolutionary history of the *nifD*, *nifK*, *nifE*, and *nifN* genes. *Journal of Molecular Evolution*, *51*, 1–11. https://doi.org/10.1007/s002390010061

Farquhar, G. D. (1982). On the nature of carbon isotope discrimination in C4 species. *Australian Journal of Plant Physiology*, *10*, 205–226.

Fleming, H., & Haselkorn, R. (1973). Differentiation in *Nostoc muscorum*: Nitrogenase is synthesized in heterocysts. *Proceedings of the National Academy of Sciences of the United States of America*, *70*, 2727–2731. https://doi.org/10.1073/pnas.70.10.2727

Flores, E., Herrero, A., Wolk, C. P., & Maldener, I. (2006). Is the periplasm continuous in filamentous multicellular cyanobacteria? *Trends in Microbiology*, *14*, 439–444. https://doi.org/10.1016/j.tim.2006.08.007

Gallon, J. R. (1992). Reconciling the incompatible: N_2 fixation and O_2. *New Phytologist*, *122*, 571–709.

Garvin, J., Buick, R., Anbar, A. D., Arnold, G. L., & Kaufman, A. J. (2009). Isotopic evidence for an aerobic nitrogen cycle in the latest Archean. *Science*, *323*, 1045–1048. https://doi.org/10.1126/science.1165675

Giovannoni, S. J., Turner, S., Olsen, G. T., Barns, S., Lane, D. J., & Pace, N. R. (1988). Evolutionary relationships among cyanobacteria and green chloroplasts. *Journal of Bacteriology*, *170*, 3584–3592. https://doi.org/10.1128/jb.170.8.3584-3592.1988

Glass, J. B., Simon-Wolfe, F., Elser, J. J., & Anbar, A. D. (2010). Molybdenum-nitrogen co-limitation in freshwater and coastal heterocystous cyanobacteria. *Limnology and Oceanography*, *55*, 667–676. https://doi.org/10.4319/lo.2009.55.2.0667

Goldblatt, C., Claire, M. W., Lenton, T. M., Matthews, A. J., Watson, A. J., & Zahnle, K. J. (2009). Nitrogen-enhanced greenhouse warming on early Earth. *Nature Geoscience*, *2*, 891–896. https://doi.org/10.1038/ngeo692

Golden, J., & Yoon, H.-S. (2003). Heterocyst development in *Anabaena*. *Current Opinion in Microbiology*, *6*, 557–563. https://doi.org/10.1016/j.mib.2003.10.004

Golubic, S., Sergeev, V. N., & Knoll, A. H. (1995). Mesoproterozoic Archaeoellipsoides: Akinetes of heterocystous cyanobacteria. *Lethaia*, *28*, 285–298. https://doi.org/10.1111/j.1502-3931.1995.tb01817.x

Guy, R. D., Reid, D. M., & Krouse, H. R. (1986). Factors affecting $^{13}C/^{12}C$ ratios of inland halophytes. I. Controlled studies on growth and isotopic composition of *Puccinella nuttalliana*. *Canadian Journal of Botany*, *64*, 2693–2699. https://doi.org/10.1139/b86-355

Hayes, J. M. (2001). Fractionation of carbon and hydrogen isotopes in biosynthetic processes. *Reviews in Mineralogy and Geochemistry*, *43*, 225–277. https://doi.org/10.2138/gsrmg.43.1.225

Hayes, J. M. (2004). An introduction to isotopic calculations. *Woods Hole Oceanographic Institution*, 1–10.

Helz, G. R., Miller, C. V., Charnock, J. M., Mosselmans, J. F. W., Pattrick, R. A. D., Garner, C. D., & Vaughan, D. J. (1996). Mechanism of molybdenum removal from the sea and its concentration in black shales: EXAFS evidence. *Geochimica et Cosmochimica Acta*, *60*, 3631–3642. https://doi.org/10.1016/0016-7037(96)00195-0

Herrero, A., Muro-Pastor, A. M., Valladares, A., & Flores, E. (2004). Cellular differentiation and the NtcA transcription factor in filamentous cyanobacteria. *FEMS Microbiology Reviews*, *28*, 469–487. https://doi.org/10.1016/j.femsre.2004.04.003

Holland, H. J., & Beukes, N. J. (1990). A paleoweathering profile from Griqualand West, South Africa: Evidence for a dramatic rise in atmospheric oxygen between 2.2 and 1.9 bybp. *American Journal of Science*, *290A*, 1–34.

Jakubek, J., Pospisil, S., Vacik, J., & Vavrik, D. (2012). *High resolution neutron imaging of microfossils*. IEEE Nuclear Science Symposium and Medical Imaging Conference Record, 226–229.

Johnson, B., & Goldblatt, C. (2017). A secular increase in continental crust nitrogen during the Precambrian. *Geochemical Perspectives Letters*, *4*, 24–28. https://doi.org/10.7185/geochemlet.1731

Johnson, B. W., & Goldblatt, C. (2018). EarthN: A new Earth system nitrogen model. *Geochemistry, Geophysics, Geosystems*, *19*, 2516–2542. https://doi.org/10.1029/2017GC007392

Kangatharalingam, N., Priscu, J. C., & Paerl, H. W. (1992). Heterocyst envelope thickness, heterocyst frequency and nitrogenase activity in *Anabaena flos-aquae*: Influence of exogenous oxygen tension. *Journal of General Microbiology*, *138*, 2673–2678. https://doi.org/10.1099/00221287-138-12-2673

Klinger, J. M., Mancinelli, R. L., & White, M. R. (1989). Biological nitrogen fixation under primordial Martian partial pressures of dinitrogen. *Advances in Space Research*, *9*, 173–176. https://doi.org/10.1016/0273-1177(89)90225-1

Klots, C. E., & Benson, B. B. (1963). Isotope effect in solution of oxygen and nitrogen in distilled water. *Journal of Chemical Physics*, *38*, 890–892. https://doi.org/10.1063/1.1733778

Knox, M., Quay, P. D., & Wilbur, D. (1992). Kinetic isotopic fractionation during air-water gas transfer of O_2, N_2, CH_4, and H_2. *Journal of Geophysical Research*, *97*, 20335–20343. https://doi.org/10.1029/92JC00949

Kopp, R. E., Kirschvink, J. L., Hilburn, I. A., & Nash, C. Z. (2005). The Paleoproterozoic snowball Earth: A climate disaster triggered by the evolution of oxygenic photosynthesis. *Proceedings of the National Academy of Sciences of the United States of America*, *102*, 11131–11136. https://doi.org/10.1073/pnas.0504878102

Kulasooriya, S., Lang, N., & Fay, P. (1972). The heterocysts of blue-green algae. III. Differentiation and nitrogenase activity. *Proceedings of the Royal Society B: Biological Sciences*, *181*, 199–209. https://doi.org/10.1098/rspb.1972.0046

Kumar, K., Mella-Herrera, R. A., & Golden, J. W. (2009). Cyanobacterial heterocysts. *Cold Spring Harbor Perspectives in Biology*, *2*, 1–19.

Laws, E. A., Popp, B. N., Bidigare, R. R., Kennicutt, M. C., & Macko, S. A. (1995). Dependence of phytoplankton carbon isotopic composition on growth rate and $[CO_2]_{aq}$: Theoretical considerations and experimental results. *Geochimica et Cosmochimica Acta*, *59*, 1131–1138. https://doi.org/10.1016/0016-7037(95)00030-4

Lee, H., Sharp, Z. D., & Fischer, T. P. (2015). Kinetic nitrogen isotope fractionation between air and dissolved N_2 in water: Implications for hydrothermal systems. *Geochemical Journal*, *49*, 571–573. https://doi.org/10.2343/geochemj.2.0380

Licari, G. R., & Cloud, P. E. (1968). Reproductive structures and taxonomic affinities of some nannofossils from the Gunflint Iron Formation. *Proceedings of the National Academy of Sciences of the United States of America*, *59*, 1053–1060. https://doi.org/10.1073/pnas.59.4.1053

Licari, G. R., & Cloud, P. (1972). Prokaryotic alga associated with Australian Proterozoic stromatolites. *Proceedings of the National Academy of Sciences of the United States of America*, *69*, 2500–2504. https://doi.org/10.1073/pnas.69.9.2500

Macko, S. A., Fogel, M. L., Hare, P. E., & Hoering, T. (1987). Isotopic fractionation of nitrogen and carbon in the synthesis of amino acids by microorganisms. *Chemical Geology: Isotope Geoscience Section*, *65*, 79–92. https://doi.org/10.1016/0168-9622(87)90064-9

Mallik, A., Li, Y., & Wiedenbeck, M. (2018). Nitrogen evolution within the Earth's atmosphere–mantle system assessed by recycling in subduction zones. *Earth and Planetary Science Letters*, *482*, 556–566. https://doi.org/10.1016/j.epsl.2017.11.045

Mariscal, V., Herrero, A., & Flores, E. (2007). Continuous periplasm in a filamentous, heterocyst-forming cyanobacterium. *Molecular Microbiology*, *65*, 1139–1145. https://doi.org/10.1111/j.1365-2958.2007.05856.x

Marty, B., Zimmerman, L., Pujol, M., Burgess, R., & Philippot, P. (2013). Nitrogen isotopic composition and density of the Archean atmosphere. *Science*, *342*, 101–104. https://doi.org/10.1126/science.1240971

Meeks, J. C., & Elhai, J. (2002). Regulation of cellular differentiation in filamentous cyanobacteria in free-living and plant-associated symbiotic growth states. *Microbiology and Molecular Biology Reviews*, *66*, 94–121. https://doi.org/10.1128/MMBR.66.1.94-121.2002

Minagawa, M., & Wada, E. (1986). Nitrogen isotope ratios of red tide organisms in the East China Sea: A characterization of biological nitrogen fixation. *Marine Chemistry*, *19*, 245–259. https://doi.org/10.1016/0304-4203(86)90026-5

Murry, M. A., Hallenbeck, P. C., & Benemann, J. R. (1984). Immunochemical evidence that nitrogenase is restricted to the heterocysts in *Anabaena cylindrica*. *Archives of Microbiology*, *137*, 194–199. https://doi.org/10.1007/BF00414542

Murry, M. A., & Wolk, C. P. (1989). Evidence that the barrier to the penetration of oxygen into heterocysts depends upon two layers of the cell envelope. *Archives of Microbiology*, *151*, 469–474. https://doi.org/10.1007/BF00454860

Nagy, L. A. (1978). New filamentous and cystous microfossils, 2,300 m.y. old, from the Transvaal Sequence. *Journal of Paleontology*, *52*, 141–154.

Navarro-Gonzalez, R., McKay, C. P., & Mvondo, D. N. (2001). A possible nitrogen crisis for Archaean life due to reduced nitrogen fixation by lightning. *Nature*, *412*, 61–64. https://doi.org/10.1038/35083537

Olson, S. L., Reinhard, C. T., & Lyons, T. W. (2016). Cyanobacterial diazotrophy and Earth's delayed oxygenation. *Frontiers in Microbiology*, *7*, 1–6.

Pang, K., Tang, Q., Chen, L., Wan, B., Niu, C., Yuan, X., & Xiao, S. (2018). Nitrogen-fixing heterocystous cyanobacteria in the Tonian Period. *Current Biology*, *28*, 616–622. https://doi.org/10.1016/j.cub.2018.01.008

Planavsky, N. J., Asael, D., Hofmann, A., Reinhard, C. T., Lalonde, S. V., Knudsen, A., … Rouxel, O. J. (2014). Evidence for oxygenic photosynthesis half a billion years before the Great Oxidation Event. *Nature Geoscience*, *7*, 283–286. https://doi.org/10.1038/ngeo2122

Planavsky, N. J., McGoldrick, P., Scott, C. T., Li, C., Reinhard, C. T., Kelly, A. E., … Lyons, T. W. (2011). Widespread iron-rich conditions in the mid-Proterozoic ocean. *Nature*, *477*, 448–451. https://doi.org/10.1038/nature10327

Popa, R., Weber, P., Pett-Ridge, J., Finzi, J., Fallon, S., Hutcheon, I., … Capone, D. (2007). Carbon and nitrogen fixation and metabolite exchange in and between individual cells of *Anabaena oscillarioides*. *International Society for Microbial Ecology*, *1*, 354–360.

R Core Team (2017). *R: A language and environment for statistical computing*. Vienna, Austria: R Foundation for Statistical Computing. Retrieved from https://www.R-project.org/

Rasmussen, B., & Buick, R. (1999). Redox state of the Archean atmosphere: Evidence from detrital heavy minerals in ca. 3250-2750 Ma sandstones from the Pilbara Craton. *Australia*. *Geology*, *27*, 115–118.

Rippka, R., Deruelles, J., Waterbury, J. B., Herdman, M., & Stanier, R. Y. (1979). Generic assignments, strain histories and properties of pure cultures of cyanobacteria. *Journal of General Microbiology*, *111*, 1–61.

Rowell, P., James, W., Smith, W. L., Handley, L. L., & Scrimgeour, C. M. (1998). ^{15}N discrimination in molybdenum- and vanadium-grown N_2-fixing *Anabaena variabilis* and *Azotobacter vinelandii*. *Soil Biology and Biochemistry*, *30*, 2177–2180. https://doi.org/10.1016/S0038-0717(98)00066-2

Sanchez-Baracaldo, P., Hayes, P. K., & Blank, C. E. (2005). Morphological and habitat evolution in the Cyanobacteria using a compartmentalization approach. *Geobiology*, *3*, 145–165. https://doi.org/10.1111/j.1472-4669.2005.00050.x

Sander, R. (2015). Compilation of Henry's law constants (version 4.0) for water as solvent. *Atmospheric Chemistry and Physics*, *15*, 4399–4981. https://doi.org/10.5194/acp-15-4399-2015

Schopf, J. W. (1968). Microflora of the Bitter Springs Formation, Late Precambrian, Central Australia. *Journal of Paleontology*, *42*, 651–688.

Schrautemeier, B., Neveling, U., & Schmitz, S. (1995). Distinct and differently regulated Mo-dependent nitrogen-fixing systems evolved for heterocysts and vegetative cells of *Anabaena variabilis* ATCC 29413: Characterization of the *fdxH1/2* gene regions as part of the *nif1/2* gene clusters. *Molecular Microbiology*, *18*, 357–369. https://doi.org/10.1111/j.1365-2958.1995.mmi_18020357.x

Sergeev, V. N. (2009). The distribution of microfossil assemblages in Proterozoic rocks. *Precambrian Research*, *173*, 212–222. https://doi.org/10.1016/j.precamres.2009.04.002

Sharma, M. (2006). Palaeobiology of Mesoproterozoic Salkhan Limestone, Semri Group, Rohtas, Bihar, India: Systematics and significance. *Journal of Earth System Science*, *115*, 67–98. https://doi.org/10.1007/BF02703027

Shen, Y., Knoll, A. H., & Walter, M. R. (2003). Evidence for low sulphate and anoxia in a mid-Proterozoic marine basin. *Nature*, *423*, 632–635. https://doi.org/10.1038/nature01651

Sigman, D. M., & Casciotti, K. L. (2001). Ocean process tracers: Nitrogen isotopes in the ocean. In J. H. Steele, K. K. Turekian, & S. A. Thorpe (Eds.), *Encyclopedia of ocean sciences* (pp. 1884–1894). New York , NY: Elsevier. https://doi.org/10.1006/rwos.2001.0172

Som, S. M., Buick, R., Hagadorn, J. W., Blake, T. S., Perreault, J. M., Harnmeijer, J. P., & Catling, D. C. (2016). Earth's air pressure billion years ago constrained to less than half of modern levels. *Nature Geoscience*, *9*, 1–5.

Som, S. M., Catling, D. C., Harnmeijer, J. P., Polivka, P. M., & Buick, R. (2012). Air density 2.7 billion years ago limited to less than twice modern levels by fossil raindrop imprints. *Nature*, *484*, 359–362. https://doi.org/10.1038/nature10890

Sra, A., Hu, Y., Martin, G., Snow, D., Ribbe, M., & Kohen, A. (2004). Competitive ^{15}N kinetic isotope effects of nitrogen-catalyzed dinitrogen reduction. *Journal of the American Chemical Society*, *126*, 12768–12769. https://doi.org/10.1021/ja0458470

Srivastava, P. (2005). Vindhyan akinites: An indicator of Mesoproterozoic biospheric evolution. *Origins of Life and Evolution of Biospheres*, *35*, 175–185. https://doi.org/10.1007/s11084-005-8765-z

Stewart, W. D. P., & Pearson, H. W. (1970). Effects of aerobic and anaerobic conditions on growth and metabolism of blue green algae. *Proceedings of the Royal Society B: Biological Sciences*, *175*, 293–311. https://doi.org/10.1098/rspb.1970.0024

Stüeken, E. E. (2013). A test of the nitrogen-limitation hypothesis for retarded eukaryote radiation: Nitrogen isotopes across a Mesoproterozoic basinal profile. *Geochimica et Cosmochimica Acta*, *120*, 121–139. https://doi.org/10.1016/j.gca.2013.06.002

Stüeken, E. E., Buick, R., Guy, B. M., & Koehler, M. C. (2015). Isotopic evidence for biological nitrogen fixation by molybdenum-nitrogenase from 3.2 Gyr. *Nature*, *520*, 666–674. https://doi.org/10.1038/nature14180

Stüeken, E. E., Kipp, M. A., Koehler, M. C., & Buick, R. (2016). The evolution of Earth's biogeochemical nitrogen cycle. *Earth-Science Reviews*, *160*, 220–239. https://doi.org/10.1016/j.earscirev.2016.07.007

Stüeken, E. E., Kipp, M. A., Koehler, M. C., Schwieterman, E. W., Johnson, B., & Buick, R. (2016). Modeling pN_2 through geological time: Implications for planetary climates and atmospheric biosignatures. *Astrobiology*, *16*, 949–963. https://doi.org/10.1089/ast.2016.1537

Thiel, T. (1993). Characterization of genes for an alternative nitrogenase in the cyanobacterium *Anabaena variabilis*. *Journal of Bacteriology*, *175*, 6276–6286. https://doi.org/10.1128/jb.175.19.6276-6286.1993

Thiel, T., & Leone, M. (1986). Effect of glutamine on growth and heterocyst differentiation in the cyanobacterium *Anabaena variabilis*. *Journal of Bacteriology*, *168*, 769–774. https://doi.org/10.1128/jb.168.2.769-774.1986

Thiel, T., Lyons, E. M., Erker, J. C., & Ernst, A. (1995). A second nitrogenase in vegetative cells of a heterocyst-forming cyanobacterium. *Proceedings of the National Academy of Sciences of the United States of America*, *92*, 9358–9362. https://doi.org/10.1073/pnas.92.20.9358

Thiel, T., & Pratte, B. (2001). Effect on heterocyst differentiation of nitrogen fixation in vegetative cells of the cyanobacterium *Anabaena variabilis* ATCC 29413. *Journal of Bacteriology*, *183*, 280–286. https://doi.org/10.1128/JB.183.1.280-286.2001

Thiel, T., & Pratte, B. S. (2014). Regulation of three nitrogenase gene clusters in the cyanobacterium *Anabaena variabilis* ATCC 29413. *Life*, *4*, 944–967. https://doi.org/10.3390/life4040944

Thomas, J. (1970). Absence of the pigments of photosystem II of photosynthesis in heterocysts of a blue-green alga. *Nature*, *228*, 181–183. https://doi.org/10.1038/228181b0

Thomazo, C., & Papineau, D. (2013). Biogeochemical cycling of nitrogen on the early Earth. *Elements*, *9*, 345–351. https://doi.org/10.2113/gselements.9.5.345

Tomitani, A., Knoll, A. H., Cavanaugh, C. M., & Ohno, T. (2006). The evolutionary diversification of cyanobacteria: Molecular– phylogenetic and paleontological perspectives. *Proceedings of the National Academy of Sciences of the United States of America*, *103*, 5442–5447. https://doi.org/10.1073/pnas.0600999103

Turner, S., Pryer, K. M., Miao, V. P. W., & Palmer, J. D. (1999). Investigating deep phylogenetic relationships among cyanobacteria and plastids by small subunit rRNA sequence analysis. *Journal of Eukaryotic Microbiology*, *46*, 327–338. https://doi.org/10.1111/j.1550-7408.1999.tb04612.x

Uyeda, J. C., Harmon, L. J., & Blank, C. E. (2016). A comprehensive study of cyanobacterial morphological and ecological evolutionary dynamics through deep geologic time. *PLoS ONE*, *11*, 1–32.

Walsby, A. E. (2007). Cyanobacterial heterocysts: Terminal pores proposed as sites of gas exchange. *Trends in Microbiology*, *15*, 340–349. https://doi.org/10.1016/j.tim.2007.06.007

Ward, B. B. (2008). Nitrification in marine systems. In D. G. Capone, D. A. Bronk, M. R. Mulholland, & E. J. Carpenter (Eds.), *Nitrogen in the marine environment* (2nd ed., pp. 199–262). New York, NY: Academic Press. https://doi.org/10.1016/B978-0-12-372522-6.00005-0

Ward, L. M., Kirschvink, J. L., & Fischer, W. W. (2016). Timescales of oxygenation following the evolution of oxygenic photosynthesis. *Origins of Life and Evolution of Biospheres*, *46*, 51–65. https://doi.org/10.1007/s11084-015-9460-3

Wei, T.-F., Ramasubramanian, T. S., & Golden, J. W. (1994). *Anabaena* sp. strain PCC 7120 *ntcA* gene required for growth on nitrate and heterocyst development. *Journal of Bacteriology*, *176*, 4473–4482. https://doi.org/10.1128/jb.176.15.4473-4482.1994

Wilcox, M., Mitchison, G. J., & Smith, R. J. (1975). Mutants of *Anabaena cylindrica* altered in heterocyst spacing. *Archives of Microbiology*, *103*, 219–223. https://doi.org/10.1007/BF00436353

Wolk, P. C. (1965). Heterocyst germination under defined conditions. *Nature*, *205*, 201–202. https://doi.org/10.1038/205201b0

Wolk, C. P., Austin, S. M., Bortins, J., & Galonsky, A. (1974). Autoradiographic localization of nitrogen gas by a heterocyst-forming blue-green alga. *The Journal of Cell Biology*, *61*(440–453).

Wolk, C. P., Thomas, J., & Shaffer, P. W. (1976). Pathway of nitrogen metabolism after fixation of ^{13}N-labeled nitrogen gas by the cyanobacterium *Anabaena cylindrica*. *The Journal of Biological Chemistry*, *251*, 5027–5034.

Yoon, H.-S. S., & Golden, J. W. (2001). PatS and products of nitrogen fixation control heterocyst pattern. *Journal of Bacteriology*, *183*, 2605–2613. https://doi.org/10.1128/JB.183.8.2605-2613.2001

Zerkle, A. L., House, C. H., Cox, R. P., & Canfield, D. E. (2006). Metal limitation of cyanobacterial N_2 fixation and implications for the Precambrian nitrogen cycle. *Geobiology*, *4*, 285–297. https://doi.org/10.1111/j.1472-4669.2006.00082.x

Zerkle, A. L., Junium, C. K., Canfield, D. E., & House, C. H. (2008). Production of ^{15}N-depleted biomass during cyanobacterial N_2-fixation at high Fe concentrations. *Journal of Geophysical Research*, *113*, 1–9.

Zhang, X., Sigman, D. M., Morel, F. M. M., & Kraepiel, A. M. L. (2014). Nitrogen isotope fractionation by alternative nitrogenases and past ocean anoxia. *Proceedings of the National Academy of Sciences of the United States of America*, *111*, 4782–4787. https://doi.org/10.1073/pnas.1402976111

SUPPORTING INFORMATION

Additional supporting information may be found online in the Supporting Information section at the end of the article.

How to cite this article: Silverman SN, Kopf SH, Bebout BM, Gordon R, Som SM. Morphological and isotopic changes of heterocystous cyanobacteria in response to N_2 partial pressure. *Geobiology*. 2018;00:1–16. https://doi.org/10.1111/gbi.12312

Supporting Information

Morphological and isotopic changes of heterocystous cyanobacteria in response to N_2 partial pressure

Silverman, Kopf, Bebout, Gordon, Som

Appendix S1: Data processing

All data (in Excel format) and source code (in R Markdown format) used to produce the figures, data tables and analyses for this paper are available online at www.github.com/KopfLab/2018_Silverman_et_al. Rendered versions of the source code are available at 2018_Silverman_et_al.kopflab.org.

Appendix S2: Heterocyst spacing

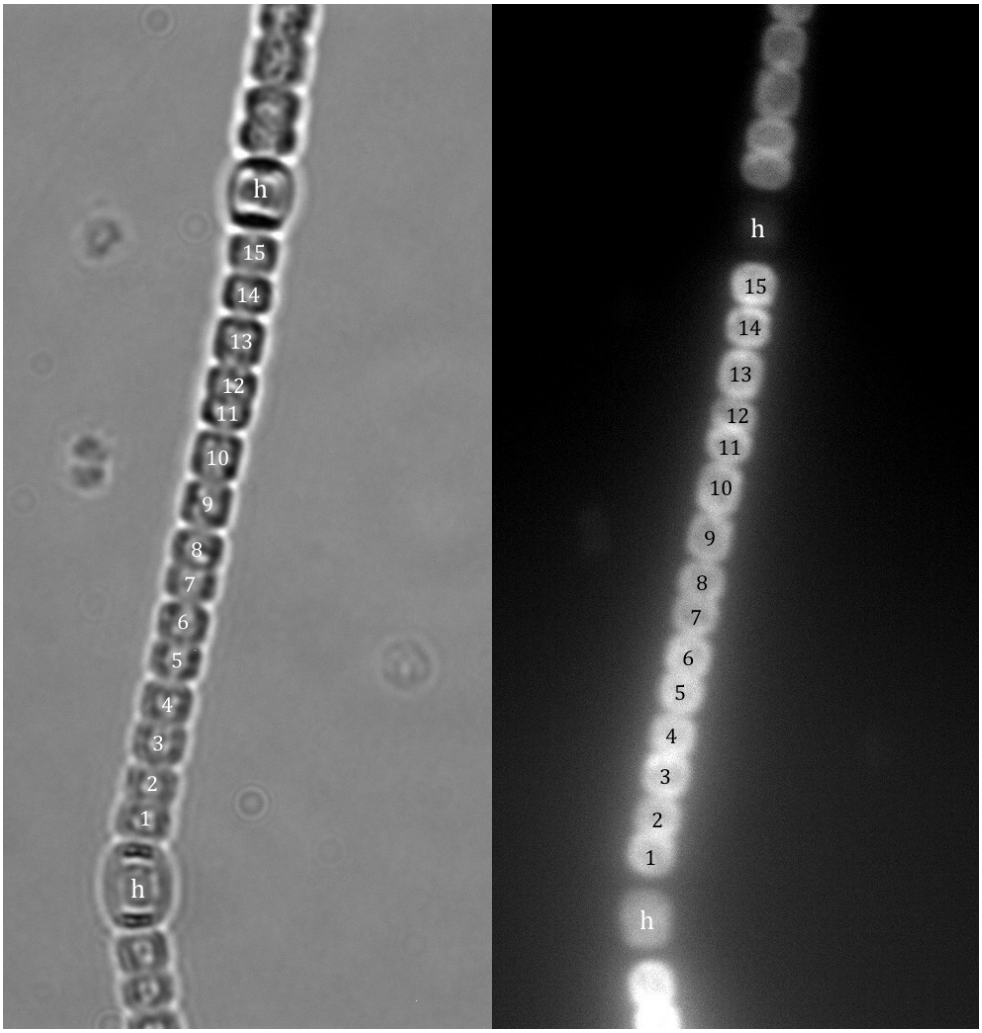

Figure S1: Example of heterocyst interval measurements. Bright-field and fluorescence micrographs of *Anabaena* filaments were used in tandem to identify heterocysts and count the number of vegetative cells (n_{cbh}= 15 here) between neighboring heterocysts (h).

Fig. S1 illustrates an example of how the heterocyst distances in all conditions were quantified. Tables S1 and S3 summarize the data represented in Figs. 4 and S2 for *A. cylindrica* and *A. variabilis*, respectively. Measurements of stationary phase heterocyst distance (n_{cbh}, number of vegetative cells between heterocysts) for each pN_2 are reported alongside the total number of heterocyst intervals counted (i.e., individual segments between two heterocysts), as well as bootstrap estimates (1000 resampled distributions) of the mean ($\bar{n}_{\mathrm{cbh}}$) and median (M_{cbh}) distances with their respective standard errors ($\pm$1 SE). Tables S2 and S4 summarize the bootstrap (1000 resamples) estimated differences ($\pm$1 SE) and significance in heterocyst distance ($\Delta\bar{n}_{\mathrm{cbh}}$) between the different experimental conditions. Reported significance levels are based on the t-test statistic of the bootstrapped distribution differences (p-value < 0.001 = ***; p-value < 0.01 = **; p-value < 0.05 = *; no significant difference: -). Using a non-parametric Wilcoxon–Mann–Whitney test on the observed distances instead of bootstrap comparisons provided identical significance levels (with p-values even slightly lower). The results show that heterocyst distances in *A. cylindrica* were significantly shorter in filaments cultivated at lower N_2 partial pressures than at higher pN_2 (i.e., p-value < 0.01 for all combinations, Table S2) while only the pN_2= 0 bar condition showed significantly shorter heterocyst distances for *A. variabilis* (i.e., all comparisons but the first column and first row of Table S4 do not show any statistically significant differences). Fig. S3 provides a comparison between the stationary phase data to other growth phases for *A. cylindrica* as described in the figure caption.

Table S1: Summary statistics of *A. cylindrica* heterocyst distances by culture growth phase in response to N_2 partial pressure. Reported errors are bootstrapped standard errors ($\pm$1 SE).

	pN_2 [bar]	segments [#]	$\bar{n}_{\mathrm{cbh}}$ [# cells]	M_{cbh} [# cells]
early-exponential	0.0	-	-	-
	0.1	643	9.33 $\pm$ 0.17	9.00 $\pm$ 0.48
	0.3	457	9.42 $\pm$ 0.20	9.00 $\pm$ 0.46
	0.5	431	11.56 $\pm$ 0.25	12.00 $\pm$ 0.54
	0.8	483	12.87 $\pm$ 0.27	12.00 $\pm$ 0.50
late-exponential	0.0	123	7.70 $\pm$ 0.31	7.00 $\pm$ 0.49
	0.1	338	11.07 $\pm$ 0.29	11.00 $\pm$ 0.40
	0.3	298	12.70 $\pm$ 0.29	12.00 $\pm$ 0.49
	0.5	370	13.87 $\pm$ 0.28	14.00 $\pm$ 0.47
	0.8	250	16.27 $\pm$ 0.47	15.00 $\pm$ 0.55
stationary	0.0	412	8.10 $\pm$ 0.18	8.00 $\pm$ 0.05
	0.1	762	10.62 $\pm$ 0.19	10.00 $\pm$ 0.48
	0.3	377	14.85 $\pm$ 0.29	14.00 $\pm$ 0.46
	0.5	250	16.94 $\pm$ 0.42	16.00 $\pm$ 0.44
	0.8	321	19.17 $\pm$ 0.45	18.00 $\pm$ 0.72

Table S2: Summary of the differences and significance in heterocyst distance ($\Delta\bar{n}_{\mathrm{cbh}}$) at different N_2 partial pressures for *A. cylindrica* in late-exponential growth phase. Reported errors are bootstrapped standard errors ($\pm$1 SE).

$\Delta\bar{n}_{\mathrm{cbh}}$	0.0 bar	0.1 bar	0.3 bar	0.5 bar	0.8 bar
0.0 bar	-	3.36 $\pm$ 0.42 (***)	4.98 $\pm$ 0.43 (***)	6.17 $\pm$ 0.42 (***)	8.56 $\pm$ 0.57 (***)
0.1 bar	-3.36 $\pm$ 0.42 (***)	-	1.61 $\pm$ 0.41 (***)	2.81 $\pm$ 0.40 (***)	5.19 $\pm$ 0.57 (***)
0.3 bar	-4.98 $\pm$ 0.43 (***)	-1.61 $\pm$ 0.41 (***)	-	1.20 $\pm$ 0.41 (**)	3.58 $\pm$ 0.55 (***)
0.5 bar	-6.17 $\pm$ 0.42 (***)	-2.81 $\pm$ 0.40 (***)	-1.20 $\pm$ 0.41 (**)	-	2.38 $\pm$ 0.54 (***)
0.8 bar	-8.56 $\pm$ 0.57 (***)	-5.19 $\pm$ 0.57 (***)	-3.58 $\pm$ 0.55 (***)	-2.38 $\pm$ 0.54 (***)	-

Table S3: Summary statistics of *A. variabilis* heterocyst distances in late-exponential growth phase in response to N_2 partial pressure. Reported errors are bootstrapped standard errors ($\pm$1 SE).

pN_2 [bar]	segments [#]	$\bar{n}_{\text{cbh}}$ [# cells]	M_{cbh} [# cells]
0.0	101	20.6 $\pm$ 1.1	21.0 $\pm$ 1.4
0.1	64	27.4 $\pm$ 2.2	25.0 $\pm$ 3.1
0.3	78	27.1 $\pm$ 1.7	26.0 $\pm$ 1.4
0.5	82	23.7 $\pm$ 1.6	23.5 $\pm$ 2.0
0.8	92	26.6 $\pm$ 1.5	26.5 $\pm$ 1.8

Table S4: Summary of the differences and significance in heterocyst distance ($\Delta\bar{n}_{\text{cbh}}$) at different N_2 partial pressures for *A. variabilis* in exponential growth phase. Reported errors are bootstrapped standard errors ($\pm$1 SE).

$\Delta\bar{n}_{\text{cbh}}$	0.0 bar	0.1 bar	0.3 bar	0.5 bar	0.8 bar
0.0 bar	-	6.8 $\pm$ 2.5 (*)	6.5 $\pm$ 2.0 (**)	3.2 $\pm$ 1.9 (-)	6.1 $\pm$ 1.9 (**)
0.1 bar	-6.8 $\pm$ 2.5 (*)	-	-0.3 $\pm$ 2.8 (-)	-3.7 $\pm$ 2.7 (-)	-0.7 $\pm$ 2.6 (-)
0.3 bar	-6.5 $\pm$ 2.0 (**)	0.3 $\pm$ 2.8 (-)	-	-3.4 $\pm$ 2.34 (-)	-0.4 $\pm$ 2.3 (-)
0.5 bar	-3.2 $\pm$ 1.9 (-)	3.7 $\pm$ 2.7 (-)	3.4 $\pm$ 2.4 (-)	-	3.0 $\pm$ 2.2 (-)
0.8 bar	-6.2 $\pm$ 1.9 (**)	0.7 $\pm$ 2.6 (-)	0.4 $\pm$ 2.3 (-)	-3.0 $\pm$ 2.2 (-)	-

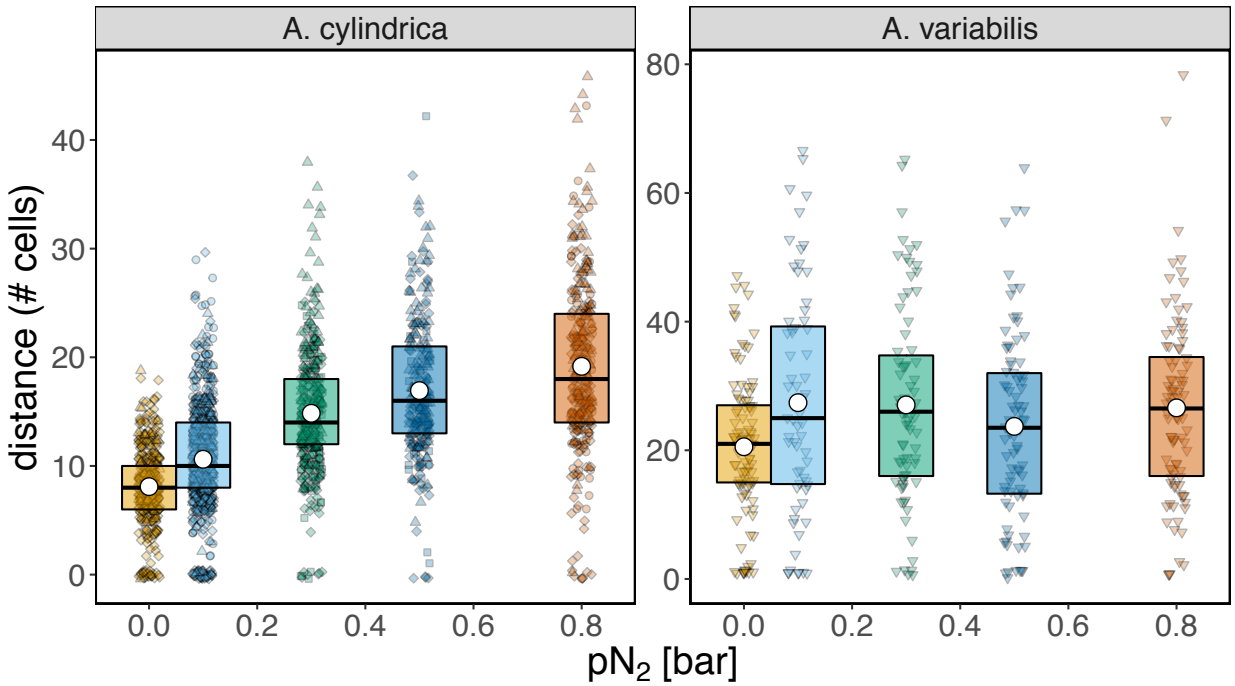

Figure S2: Exponential phase heterocyst distances in response to pN_2 for *A. cylindrica* and *A. variabilis*. Cultures were induced to develop heterocysts in nitrogen-free BG-11_0 media under different N_2 partial pressures, and heterocyst distances were measured in exponential phase by microscopy. Each recorded heterocyst distance is represented by an individual data point; symbols distinguish individual experiments conducted. The distribution of heterocyst distances for each pN_2 is shown as a box plot with the mean (circle), median (center line), and 50% interquartile range (box height). These data are summarized with the bootstrapped means and error of the means in the main text (Fig. 4).

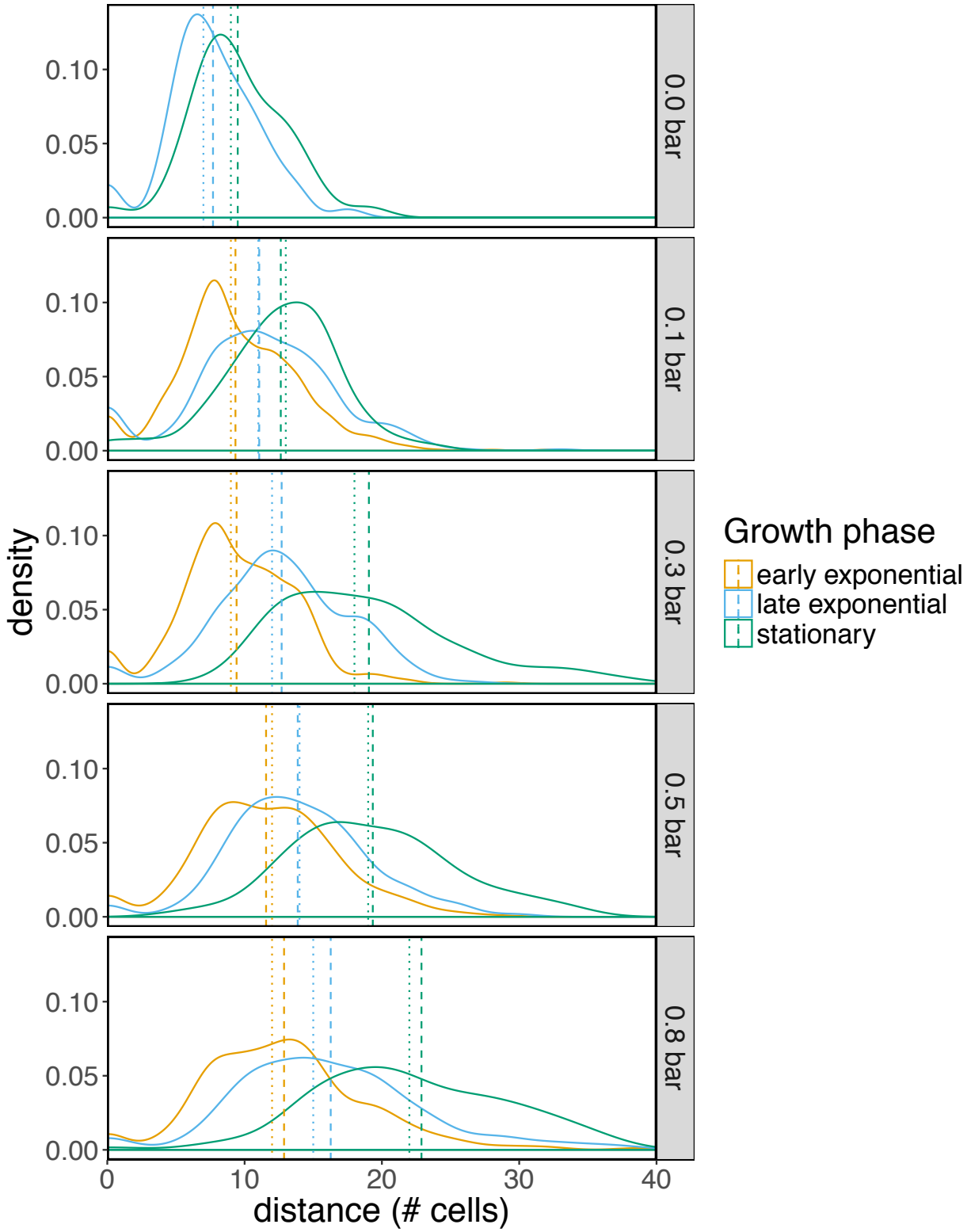

Figure S3: Comparison of heterocyst distances at different growth phases of *Anabaena cylindrica*. Cultures were induced to develop heterocysts in nitrogen-free BG-11_0 media under different N_2 partial pressures and were sampled at t=4 d (early-exponential phase), 7 d (late-exponential phase) and 15 d (stationary phase). See growth curves in Fig. S5 for corresponding optical densities. Heterocyst distances were measured by microscopy and are visualized here as density curves. In descending vertical order of the panels: pN_2 = 0, 0.1, 0.3, 0.5 and 0.8 bar. Despite biological variation in the different growth phases, the mean (dashed lines) and median (dotted lines) heterocyst distances increased with pN_2 at all three time points.

Appendix S3: Growth curves and growth rate estimates

A. cylindrica cultures were grown in nitrate-containing BG-11 under two different N_2 partial pressures and showed nearly identical growth (Fig. S4), indicating pN_2 does not affect culture growth when the cells are not fixing N_2. In contrast, the growth patterns of *A. cylindrica* and *A. variabilis* were significantly affected by pN_2 (Fig. S5). Optical density data was assumed to be most reliable as a relative proxy for biomass at OD_{750} values up to 0.4 (a conservative upper limit for the linearity of optical density measurements) as indicated by the black horizontal lines in Fig. S5. Maximum growth rates (μ) were estimated from the OD_{750} data in this interval with a log-linear regression model (vs. time t) based on the following equations:

- Exponential growth equation for biomass (B): $B(t) = B_{t0} \cdot e^{\mu t}$
- Linear relationship between OD_{750} and biomass with some proportionality factor k: $\mathrm{OD}_{750} = k \cdot B$
- Resulting linear regression model: $\ln\left(\frac{B(t)}{B_0}\right) = \mu \cdot t \rightarrow \ln\left(\frac{\mathrm{OD}_{750}(t)}{\mathrm{OD}_{750}(t_0)}\right) = \mu \cdot t$

The calculated growth rates (slopes of the regression) were bootstrapped with 1000 resamplings of the original OD data to estimate mean growth rates and standard errors for each experimental condition. Fig. S6 summarizes the growth rates showing that both species of *Anabaena* grew more slowly at $pN_2 < 0.5$ bar but showed no statistically significant growth inhibition at 0.5 bar and above. These growth rate data were used in the isotope fractionation and enzyme kinetic models presented in Appendix S5: and Appendix S6:.

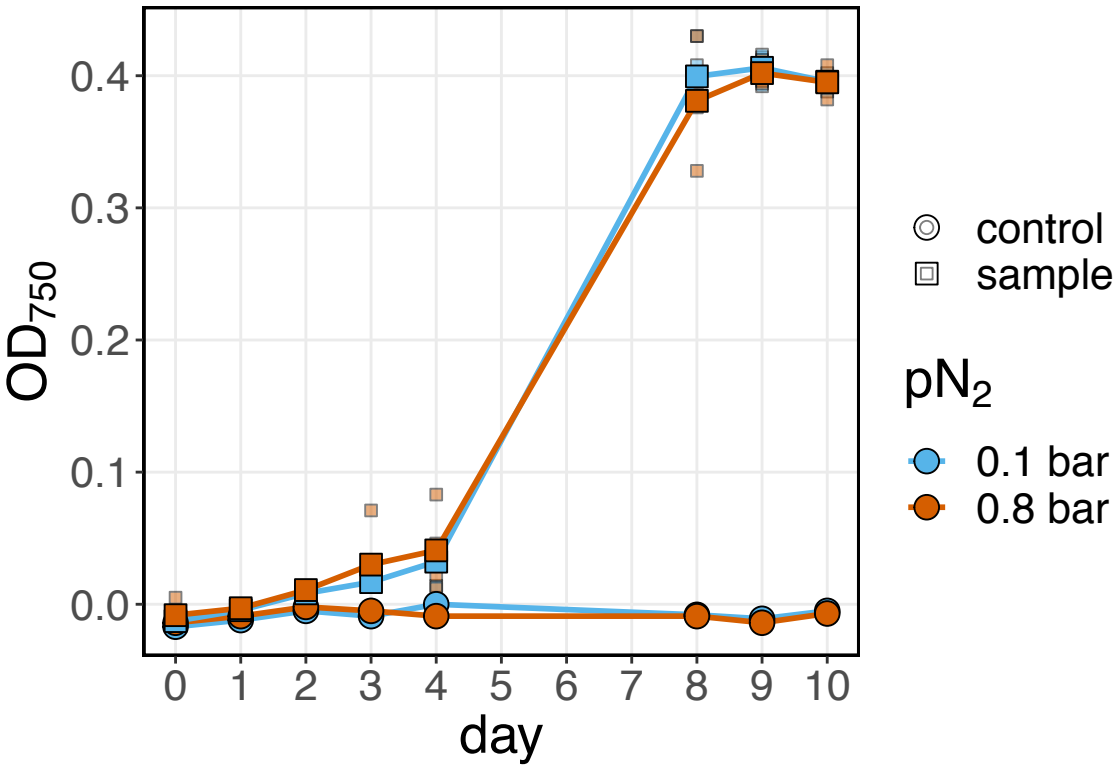

Figure S4: Optical density at 750 nm (OD_{750}) of *Anabaena cylindrica* grown in nitrate-rich BG-11 under 0.1 and 0.8 bar N_2. In absence of nitrogen-fixing conditions, culture growth is not affected by pN_2.

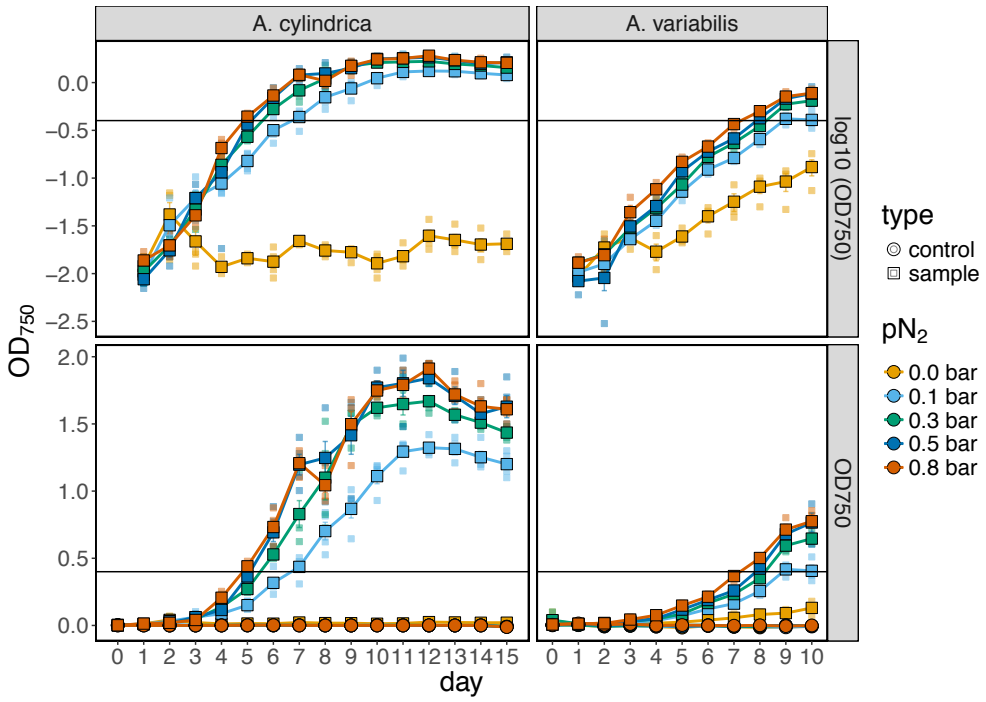

Figure S5: Optical density at 750 nm (OD_{750}) of *Anabaena* sp. grown in BG-11_0 under different pN_2 conditions. Top panels show OD_{750} on logarithmic scale, bottom panels on linear scale. Lines connect bootstrapped averages of biological replicates with smaller symbols showing individual data points. Errors bars are bootstrapped standard errors ($\pm$1 SE) and may be smaller than symbol sizes. Black horizontal lines show optical density cutoff (OD_{750}= 0.4) for growth rate calculations.

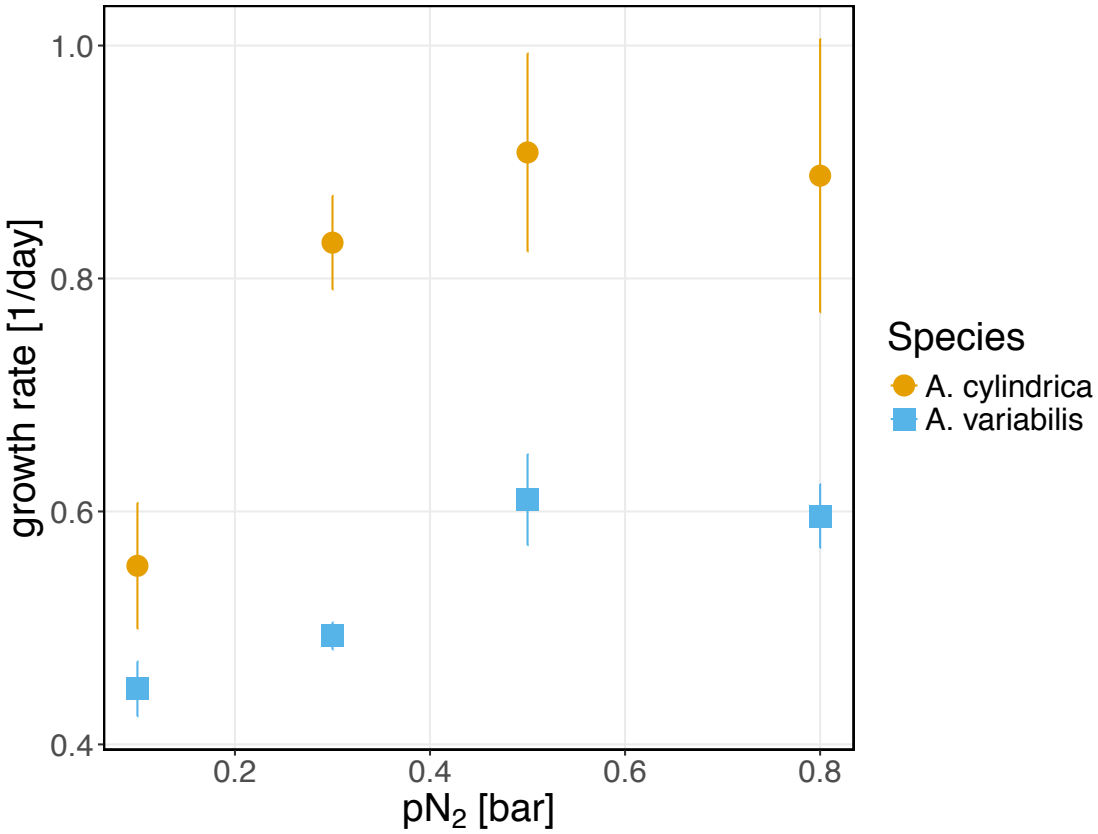

Figure S6: Growth rates of *Anabaena cylindrica* (circles) and *Anabaena variabilis* (squares) grown under different pN_2 conditions. Data points are bootstrapped averages based on regression analyses of the data from initial log phases of the growth curves in Fig. S5. Errors bars are bootstrapped standard errors ($\pm$1 SE).

Appendix S4: Experimental pH, O_2 and CO_2 variation

Preliminary growth experiments were carried out to test the growth yield, and pH and O_2 variations of *A. cylindrica* with the total inorganic carbon available from one flushing of the headspace. The experimental system in this study consists of 25 ml anaerobic culture tubes with 10 ml of medium initially adjusted to a pH of 7.8 in the presence of 20 mM HEPES (pKa = 7.5), and 15 ml of headspace under atmospheric CO_2 conditions (~400 ppm) at room temperature. Upon quick flushing of the headspace with different gas mixtures that contain 0.2 bar CO_2, the total inorganic carbon is increased, which leads to a decrease in pH. As the inorganic carbon is consumed through photosynthetic activity, the pH increases again. Efficient equilibration between the headspace and liquid during growth is achieved by continuous agitation.

The available carbon from one headspace sparging enabled the cultures to grow to an optical density of ~0.4 (panel A in Fig. S7). Inorganic carbon and pH are calculated for these preliminary experiments based on carbonate chemistry, with general equilibrium equations of the carbonate system as follows (assuming STP):

$$\text{dissociation of carbonic acid: } \mathrm{H_2CO_3^*} \rightleftharpoons \mathrm{H^+}+\mathrm{HCO_3^-}$$

$$\text{with dissociation constant } \frac{[\mathrm{H^+}][\mathrm{HCO_3^-}]}{[\mathrm{H_2CO_3^*}]} = K_1 = 10^{-6.3}$$

$$\text{dissociation of bicarbonate: } \mathrm{HCO_3^-} \rightleftharpoons \mathrm{H^+}+\mathrm{CO_3^{2-}}$$

$$\text{with dissociation constant } \frac{[\mathrm{H^+}][\mathrm{CO_3^{2-}}]}{[\mathrm{HCO_3^-}]} = K_2 = 10^{-10.3}$$

$$\text{water dissociation: } \mathrm{H_2O} \rightleftharpoons \mathrm{H^+}+\mathrm{OH^-}$$

$$\text{with dissociation constant } [\mathrm{H^+}][\mathrm{OH^-}] = K_\mathrm{w} = 10^{-14}$$

$$\text{dissolved inorganic carbon (DIC): } [\mathrm{DIC}]=[\mathrm{H_2CO_3^*}]+[\mathrm{HCO_3^-}]+[\mathrm{CO_3^{2-}}]$$

$$\text{charge balance (not considering any other solutes): } [\mathrm{H^+}]\text{-}[\mathrm{HCO_3^-}]\text{-}2\cdot[\mathrm{CO_3^{2-}}]\text{-}[\mathrm{OH^-}]=0$$

Besides the carbonate system, both the basicity from the addition of sodium hydroxide (adding $[\mathrm{Na^+}]$ and $[\mathrm{OH^-}]$ during initial pH adjustment) and any dissociated pH buffer (here the portion of the total HEPES, $[A_\mathrm{T}]$ for short, that is dissociated into $[\mathrm{A^-}]$ and $[\mathrm{H^+}]$ with acid dissociation constant $K_\mathrm{a} = \frac{[\mathrm{A^-}][\mathrm{H^+}]}{[\mathrm{AH}]}$ and mass balance $[A_\mathrm{T}] = [\mathrm{AH}] + [\mathrm{A^-}]$) contribute to the overall charge balance (note that the second dissociation of HEPES around pH 3 is not significant at the circumneutral pHs considered here and thus omitted for clarity):

$$[\mathrm{H^+}]\text{-}[\mathrm{HCO_3^-}]\text{-}2\cdot[\mathrm{HCO_3^{2-}}]\text{-}[\mathrm{OH^-}]\text{-}[\mathrm{A^-}]+[\mathrm{Na^+}]=0$$

CO_2 is moderately soluble in water forming aqueous CO_2 and hydrated carbonic acid with a Henry's law constant of $K_\mathrm{H} = 3.3 \cdot 10^{-4} \frac{\mathrm{mol}}{\mathrm{m^3Pa}} = 0.033 \frac{\mathrm{M}}{\mathrm{atm}}$ at $\mathrm{T} = 298.15\mathrm{K}$ (25°C). Substituting in all relevant acid dissociation and gas dissolution constants (K_x) yields the following equation:

$$[\mathrm{H^+}]+[\mathrm{Na^+}]\text{-}\frac{K_\mathrm{a}\cdot[A_\mathrm{T}]}{K_\mathrm{a}+[\mathrm{H^+}]}\text{-}\frac{K_1 K_\mathrm{H}\cdot\mathrm{pCO_2}}{[\mathrm{H^+}]}\text{-}2\frac{K_1 K_2 K_\mathrm{H}\cdot\mathrm{pCO_2}}{[\mathrm{H^+}]^2}\text{-}\frac{K_\mathrm{w}}{[\mathrm{H^+}]}=0$$

where K_H is Henry's law constant. For a closed system such as the one used in this study (stoppered culture tubes), the mass balance based on total moles of carbon in the entire system provides an additional constraint.

Total inorganic carbon (C_T) can be mass balanced using the ideal gas law and relevant acid dissociation and gas dissolution constants:

$$
\begin{aligned}
C_\mathrm{T} &= n_{\mathrm{CO_2}(g)} + V_\mathrm{liquid} \cdot \mathrm{DIC} \\
\mathrm{DIC} &= [\mathrm{H_2CO_3^*}]+[\mathrm{HCO_3^-}]+[\mathrm{CO_3^{2-}}]=K_\mathrm{H} \cdot \mathrm{pCO_2} \left(1 + \frac{K_1}{[\mathrm{H^+}]} + \frac{K_1 K_2}{[\mathrm{H^+}]^2}\right) \\
n_{\mathrm{CO_2(g)}} &= \frac{\mathrm{pCO_2} \cdot V_\mathrm{headspace}}{\mathrm{RT}} \\
C_\mathrm{T} &= \mathrm{pCO_2} \cdot \left[\frac{V_\mathrm{headspace}}{\mathrm{RT}} + V_\mathrm{liquid} \cdot K_\mathrm{H} \left(1 + \frac{K_1}{[\mathrm{H^+}]} + \frac{K_1 K_2}{[\mathrm{H^+}]^2}\right)\right]
\end{aligned}
$$

With these constraints, a final equation relating pH to the added base $[\mathrm{Na^+}]$, total buffer $[A_\mathrm{T}]$, total inorganic carbon (C_T) and headspace + liquid volume in the system can be derived and solved for pH by standard numerical root-finding algorithms.

$$
[\mathrm{H^+}]+[\mathrm{Na^+}]\text{-}\frac{K_\mathrm{a}}{K_\mathrm{a} + [\mathrm{H^+}]} \cdot [A_\mathrm{T}]\text{-}\frac{\frac{K_1}{[\mathrm{H^+}]} + 2\frac{K_1 K_2}{[\mathrm{H^+}]^2}}{\frac{V_\mathrm{headspace}}{K_\mathrm{H} \cdot \mathrm{RT}} + \left(1 + \frac{K_1}{[\mathrm{H^+}]} + \frac{K_1 K_2}{[\mathrm{H^+}]^2}\right) V_\mathrm{liquid}} \cdot C_\mathrm{T}\text{-}\frac{K_\mathrm{w}}{[\mathrm{H^+}]}
$$

$$
10^{-\mathrm{pH}} + [\mathrm{Na^+}] - \frac{1}{1 + 10^{(\mathrm{p}K_a - \mathrm{pH})}} \cdot [A_\mathrm{T}] - \frac{10^{(\mathrm{pH} - \mathrm{p}K_1)} + 2 \cdot 10^{(2 \cdot \mathrm{pH} - \mathrm{p}K_1 - \mathrm{p}K_2)}}{\frac{V_\mathrm{headspace}}{K_\mathrm{H} \cdot \mathrm{RT}} + (1 + 10^{(\mathrm{pH} - \mathrm{p}K_1)} + 10^{(2 \cdot \mathrm{pH} - \mathrm{p}K_1 - \mathrm{p}K_2)}) V_\mathrm{liquid}} \cdot C_\mathrm{T} - 10^{(\mathrm{pH} - \mathrm{p}K_\mathrm{w})} = 0
$$

In parallel to the pH increase as during inorganic carbon consumption through photosynthesis, molecular oxygen ($\mathrm{O_2}$) is produced with the 1:1 stoichiometry of photosynthesis ($\mathrm{CO_2}+\mathrm{H_2O} \rightarrow \mathrm{O_2}+\mathrm{CH_2O}$). $\mathrm{O_2}$ is sparingly soluble in water and distributes between the liquid and gas phase according to the Henry's law constant for $\mathrm{O_2}$: $K_\mathrm{H} = 1.3 \cdot 10^{-5} \frac{\mathrm{mol}}{\mathrm{m^3 Pa}} = 0.0013 \frac{\mathrm{M}}{\mathrm{atm}}$ at $\mathrm{T} = 298.15\mathrm{K}$ (25°C). The equations for closed system $\mathrm{O_2}$ are as follows:

$$
\begin{aligned}
\mathrm{O_{2(total)}} &= n_{\mathrm{O_2(g)}} + V_\mathrm{liquid} \cdot [\mathrm{O_{2(aq)}}] = \frac{\mathrm{pO_2} \cdot V_\mathrm{headspace}}{\mathrm{RT}} + K_\mathrm{H} \cdot \mathrm{pO_2} \cdot V_\mathrm{liquid} \\
\rightarrow \mathrm{pO_2} &= \frac{\mathrm{O_{2(total)}}}{\frac{V_\mathrm{headspace}}{\mathrm{RT}} + K_\mathrm{H} \cdot V_\mathrm{liquid}}
\end{aligned}
$$

$\mathrm{pO_2}$ was confirmed at the end of the experiment. Top and bottom figures of panel B (Fig. S7) illustrate the pH and $\mathrm{O_2}$ variations that can result after an inorganic carbon spike. Given these variations, a semi-continuous culture setup with daily headspace sparging was used for main experiments to ensure $\mathrm{CO_2}$ did not run out and $\mathrm{O_2}$ did not build up to inhibitory levels to nitrogenase.

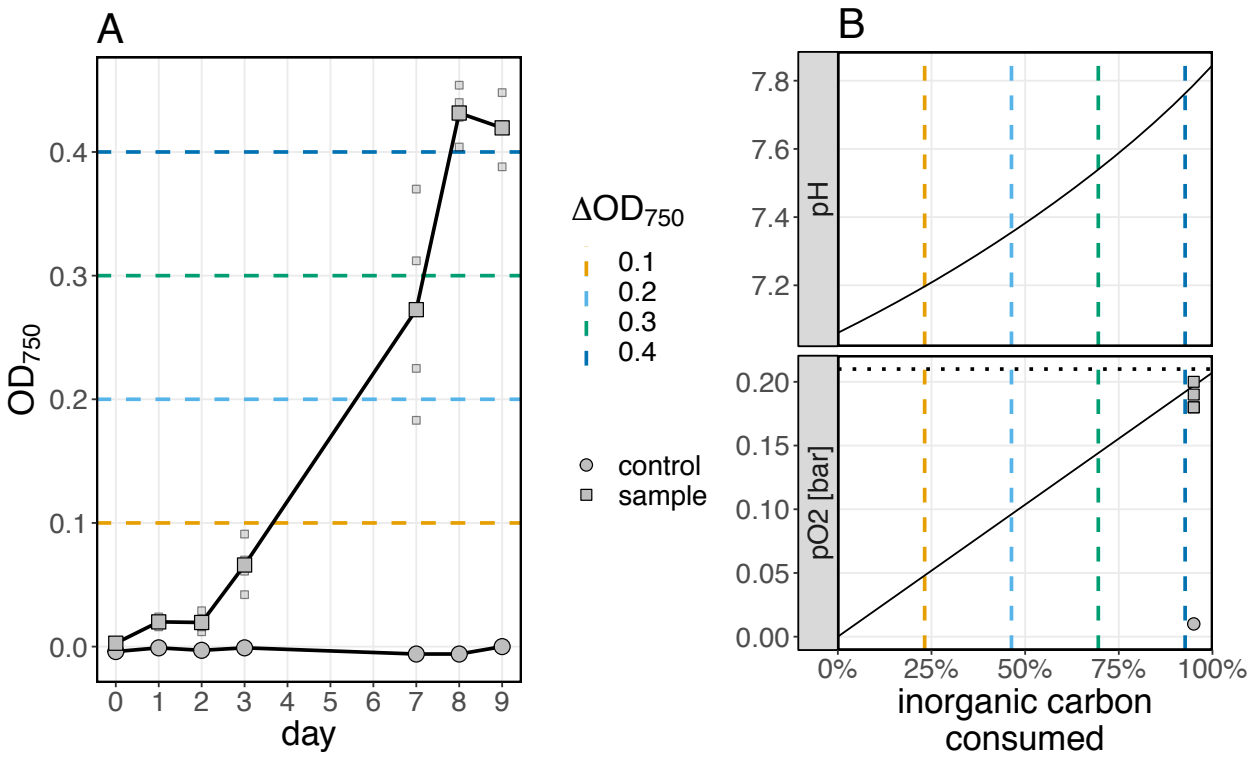

Figure S7: Growth yield, and pH and O_2 variations of *Anabaena cylindrica* cultivated in BG-11_0 under headspace sparged once with 0.5 bar pN_2 and 0.2 bar CO_2. (A) Available carbon sustained culture growth to OD_{750} of ~0.4. (B) pH and pO_2 increased predictably per 0.1 OD_{750} increment as total inorganic carbon was depleted.

Appendix S5: Isotope data and fractionation model

Data

Fig. S8 and Table S5 summarize the measured fractionation factors for *A. cylindrica* and *A. variabilis* from this study. Fig. S9 shows the calibration regressions for correction of raw isotope data.

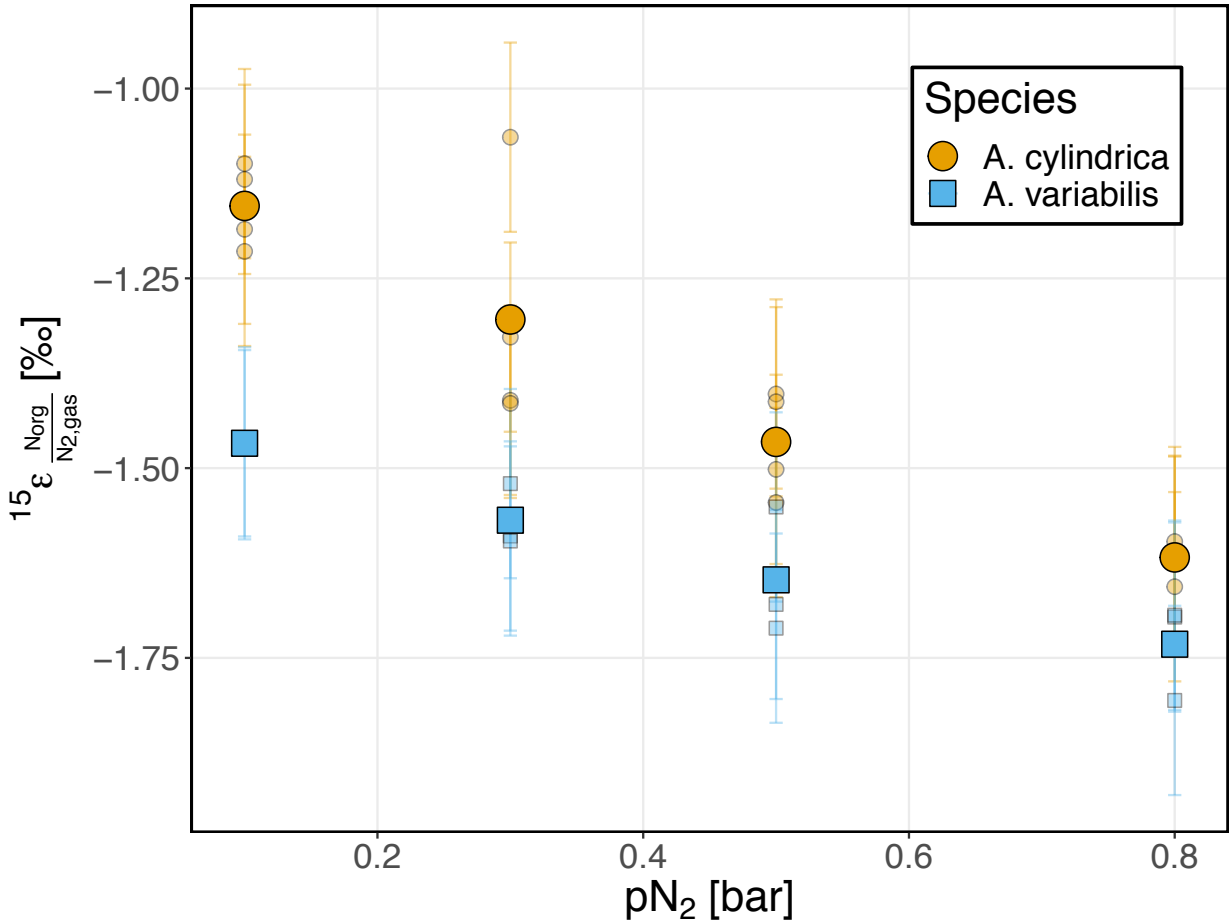

Figure S8: Overview of all biological replicates (small data points) of the isotope fractionation factors (ϵ^{15}N) measured between biomass and N_2 for *Anabaena cylindrica* (circles) and *Anabaena variabilis* (squares) cultivated under different N_2 partial pressures. Large data points represent averages. Error bars show analytical precision (σ_a).

Table S5: Summary of the average isotope fractionation factors (ϵ^{15}N, in ‰ vs. air N_2) between biomass and N_2 from biological replicates of *Anabaena cylindrica* and *Anabaena variabilis* cultivated under different N_2 partial pressures. Reported errors of the means are bootstrapped standard errors (±1 SE). σ_a indicates the analytical precision. The absolute systematic uncertainty on all measurements is 0.3‰ based on the uncertainty of the employed reference material. These data are shown visually in the main text in Fig. 4.

Species	pN_2 [bar]	biological replicates	$\epsilon^{15}N_{Norg/N2.gas}$ [‰]	σ_a [‰]
A. cylindrica	0.1	4	-1.15 ± 0.02	± 0.12
A. cylindrica	0.3	4	-1.31 ± 0.07	± 0.12
A. cylindrica	0.5	4	-1.47 ± 0.03	± 0.12
A. cylindrica	0.8	4	-1.62 ± 0.01	± 0.12
A. variabilis	0.1	2	-1.47 ± 0.00	± 0.12
A. variabilis	0.3	3	-1.57 ± 0.02	± 0.12
A. variabilis	0.5	3	-1.65 ± 0.04	± 0.12
A. variabilis	0.8	3	-1.73 ± 0.03	± 0.12

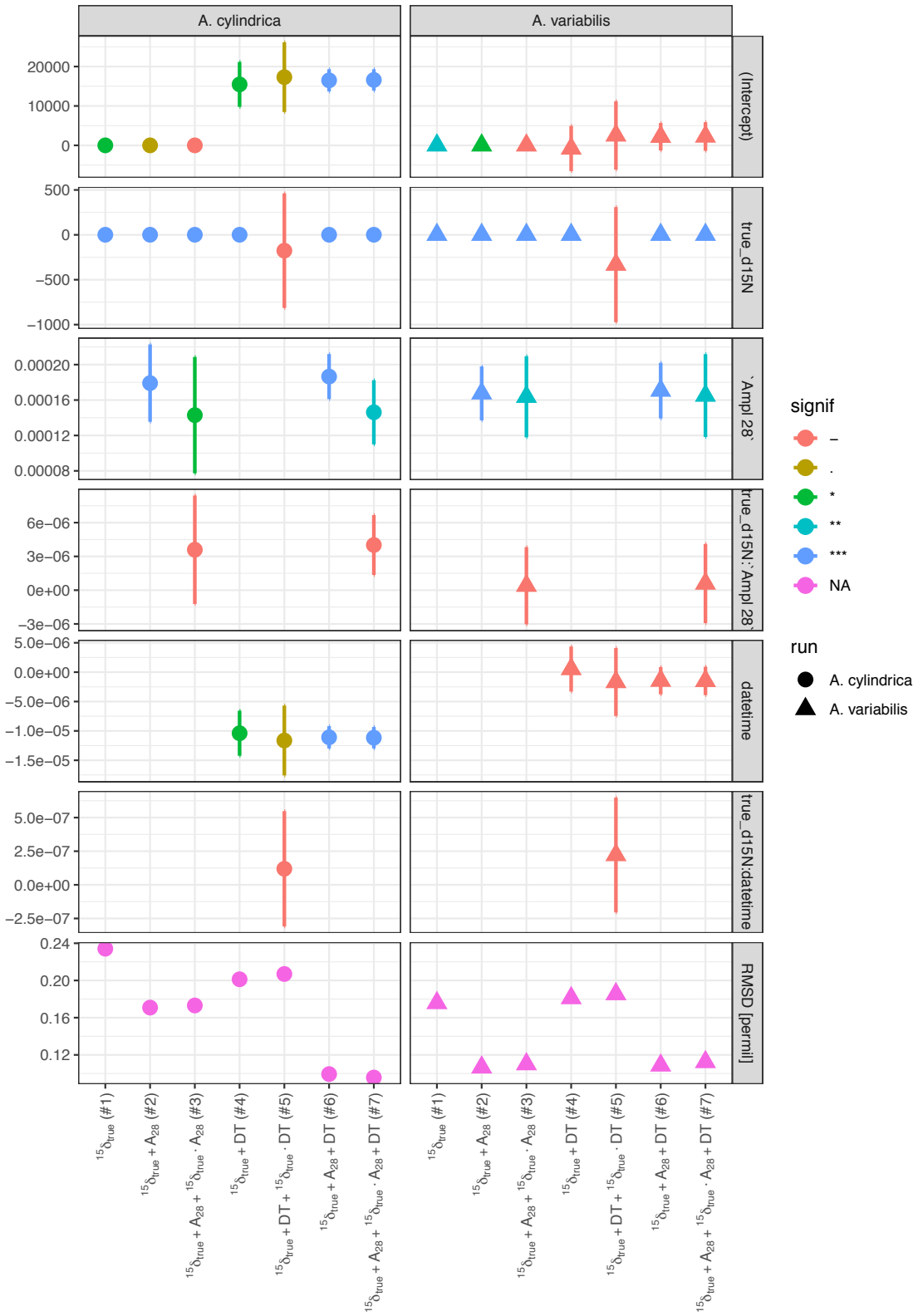

Figure S9: Visualization of calibration regressions for correction of isotope data. Calibration models were run across all isotope standards (detailed in Materials and Methods) evaluating individual parameters to gain a better understanding of their individual contributions and relevance. Regression models tested are numbered across the bottom of the figure and consider the following parameters: isotopic value ($^{15}\delta_{\mathrm{true}}$), signal intensity ($A_{28}$, i.e. amplitude), temporal drift (DT, i.e. datetime), and their cross effects. The simplest combination of parameters that shows statistical significance (i.e. lowest residual mean standard deviation, or RMSD) is the model that best explains the variance in standards (model #6 for *A. cylindrica* (left) and #2 for *A. variabilis* (right), highlighted by the rectangles) and was used to correct the isotopic data.

Isotope fractionation model

This section describes the isotopic flux model used to contextualize the data (as shown in Fig. 7) and provides details on its derivation.

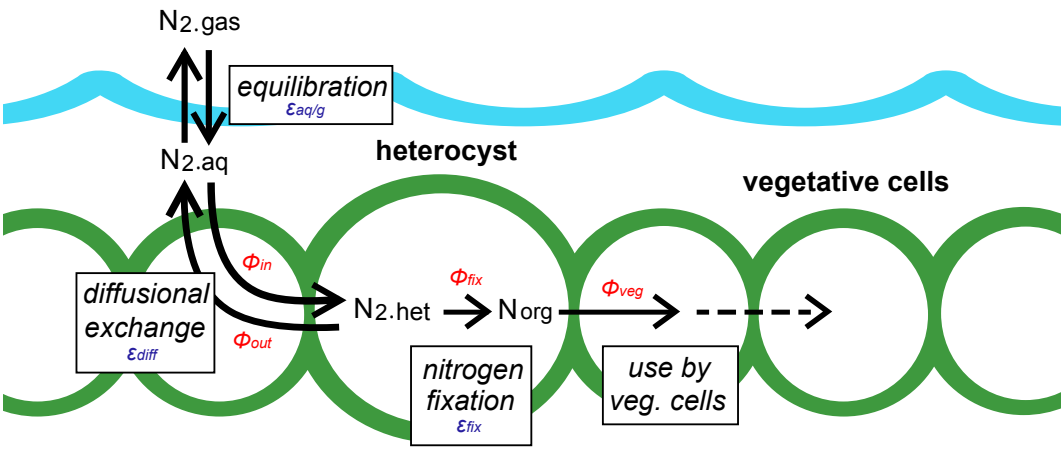

Figure S10: Steady state flux model for the nitrogen isotope fractionation during nitrogen fixation. Same as Fig. 2 with fluxes added in red and fractionation factors in blue for easy reference.

Following the approach employed by Laws et al. (1995) to understand the growth-rate dependent organismal isotope effect during carbon fixation, we developed a quasi steady-state model (Hayes, 2004) for the organismal isotope effect of nitrogen fixation in heterocystous cyanobacterial filaments, as outlined below.

Flux balance

Assuming a quasi steady-state flux of nitrogen through *Anabaena* filaments, N_2 fixed by nitrogenase in the heterocysts (ϕ_{fix}) and delivered to the vegetative cells (ϕ_{veg}) must balance the flux of N_2 in (ϕ_{in}) and out (ϕ_{out}) of the heterocysts. Exchange of N_2 is thought to occur primarily by diffusion through the pores between the vegetative cells and heterocysts (Fig. S10), so the flux of N_2 that enters the heterocyst is proportional to the external concentration of N_2 ($C_{\mathrm{N2.out}}$), while the flux of N_2 that leaves the heterocyst is proportional to the concentration of N_2 within the heterocyst ($C_{\mathrm{N2.het}}$). Dissolved $N_{2.\mathrm{aq}}$ (i.e. $C_{\mathrm{N2.out}}$) is assumed to remain in equilibrium with the virtually infinite reservoir of gaseous $N_{2.\mathrm{gas}}$ ($\mathrm{pN_2}$) in the headspace, with the proportionality between them described by Henry's law ($\mathrm{C_{N2.out}}{=}K_{\mathrm{H}}{\cdot}\mathrm{pN_2}$; solubility constant K_{H} for N_2 gas in water is $6.5{\times}10^{-4}$ mol L^{-1} bar^{-1}, Sander, 2015). This leads to the following set of flux equations:

$$
\begin{aligned}
\phi_{\mathsf{veg}} &= \phi_{\mathsf{fix}} \\
\phi_{\mathsf{fix}} &= \phi_{\mathsf{in}} - \phi_{\mathsf{out}} \\
\phi_{\mathsf{out}} &= K_2 \cdot C_{\mathsf{N2.het}} \\
\phi_{\mathsf{in}} &= K_1 \cdot C_{\mathsf{N2.out}} = K_1 \cdot K_{\mathrm{H}} \cdot \mathrm{pN_2}
\end{aligned}
\tag{S1}
$$

The corresponding isotope flux balances are as follows, with all δ and ϵ values referring to the nitrogen isotope system (errors from mass balance calculations in δ space are assumed to be negligible given the small isotopic

effects; Hayes, 2004):

$$\begin{aligned} \phi_{\text{veg}} \cdot \delta_{\phi\text{veg}} &= \phi_{\text{fix}} \cdot \delta_{\phi\text{fix}} \\ \phi_{\text{fix}} \cdot \delta_{\phi\text{fix}} &= \phi_{\text{in}} \cdot \delta_{\phi\text{in}} - \phi_{\text{out}} \cdot \delta_{\phi\text{out}} \end{aligned} \tag{S2}$$

The isotopic composition of the fluxes ($\delta_{\phi\text{x}}$) can be described as follows, with $\epsilon_{\text{aq/g}}$ as the equilibrium fractionation factor between the aqueous and gaseous phase of N_2; ϵ_{diff} the kinetic isotope fractionation factor of N_2 diffusion through the aqueous medium and cells; and ϵ_{fix} the intrinsic kinetic isotope fractionation factor of nitrogenase during the nitrogen fixation reaction (see Fig. S10 for visualization of the fluxes and reservoirs):

$$\begin{aligned} \delta_{\phi\text{veg}} &= \delta_{\text{Norg}} \\ \delta_{\phi\text{fix}} &= \delta_{\text{N2.het}} - \varepsilon_{\text{fix}} \\ \delta_{\phi\text{out}} &= \delta_{\text{N2.het}} - \varepsilon_{\text{diff}} \\ \delta_{\phi\text{in}} &= \delta_{\text{N2.gas}} + \varepsilon_{\frac{\text{aq}}{g}} - \varepsilon_{\text{diff}} \end{aligned} \tag{S3}$$

All kinetic fractionation factors are defined as ${}^{15}\epsilon_{\frac{\text{Norg}}{\text{N2.gas}}} = \left[\left(\frac{^{15}\text{N}}{^{14}\text{N}}\right)_{\text{N}_{\text{org}}} / \left(\frac{^{15}\text{N}}{^{14}\text{N}}\right)_{\text{N}_{2.\text{gas}}} - 1\right] \times 1000$ as discussed in the Materials and Methods. As indicated by Eq. S3, the isotopic composition of the N_2 entering the heterocyst ($\delta_{\phi_{\text{in}}}$) depends on the isotopic composition of the gaseous N_2 in the headspace or atmosphere ($\delta_{\text{N2.gas}}$) in equilibrium with the aqueous N_2 reservoir, $\epsilon_{\text{aq/g}}$ and ϵ_{diff}; the isotopic composition of the fixed nitrogen ($\delta_{\phi_{\text{fix}}}$) depends on the isotopic composition of N_2 inside the heterocyst ($\delta_{\text{N2.het}}$) and ϵ_{fix}. The isotopic composition of the N_2 exiting the heterocyst ($\delta_{\phi_{\text{out}}}$) depends on $\delta_{\text{N2.het}}$ and ϵ_{diff}. Combining Eqs. S1, S2 and S3 leads to the following expression for the overall organismal fractionation factor between organic nitrogen and N_2 gas ($\varepsilon_{\text{Norg/N2.gas}}$):

$$\varepsilon_{\frac{\text{Norg}}{\text{N2.gas}}} = \delta_{\text{Norg}} - \delta_{\text{N2.gas}} = \varepsilon_{\frac{\text{aq}}{g}} - \varepsilon_{\text{diff}} + (\varepsilon_{\text{diff}} - \varepsilon_{\text{fix}}) \frac{K_2 \cdot C_{\text{N2.het}}}{K_1 \cdot K_{\text{H}} \cdot \text{pN}_2} \tag{S4}$$

Growth constraints

Because nitrogen is the sole limiting nutrient in this system, the steady-state growth rate (μ) of the vegetative cells ($\mu \cdot n_{veg}$) must be proportional to the total flux of nitrogen fixed ($\phi_{\text{fix.total}}$). In the case of *A. cylindrica*, nitrogen fixation is confined to the heterocysts, so $\phi_{\text{fix.total}}$ can be inferred from the number of heterocysts (n_{het}) and the average nitrogen fixation flux per heterocyst (ϕ_{fix}), leading to the following set of equations (with yield constant K_{Y} for biomass growth):

$$\begin{aligned} \phi_{\text{fix.total}} &= \phi_{\text{fix}} \cdot n_{\text{het}} \\ \mu \cdot n_{\text{veg}} &= K_{\text{Y}} \cdot \phi_{\text{fix.total}} = K_{\text{Y}} \cdot \phi_{\text{fix}} \cdot n_{\text{het}} \end{aligned} \tag{S5}$$

The ratio of vegetative to heterocyst cells ($\frac{n_{\text{veg}}}{n_{\text{het}}}$) can be more intuitively represented as the *number of vegetative cells between heterocysts* (n_{cbh}), which is used to represent data for the heterocyst intervals (see Figs. 4 and S2). Combining Eq. S5 with the fluxes from Eq. S1 to eliminate ϕ_{fix} gives the following expression:

$$\mu = K_{\text{Y}} \cdot \frac{K_1 \cdot K_{\text{H}} \cdot \text{pN}_2 - K_2 \cdot C_{\text{N2.het}}}{n_{\text{cbh}}} \tag{S6}$$

Eq. S6 can be combined with Eq. S4 to eliminate $C_{\mathrm{N2.het}}$ and yield the following expression for $\varepsilon_{\mathrm{Norg/N2.gas}}$:

$$\varepsilon_{\frac{\mathrm{Norg}}{\mathrm{N2.gas}}} = \varepsilon_{\frac{\mathrm{aq}}{g}} - \varepsilon_{\mathrm{diff}} - (\varepsilon_{\mathrm{diff}} - \varepsilon_{\mathrm{fix}}) \left(1 - \frac{1}{K_1 \cdot K_{\mathrm{Y}} \cdot K_{\mathrm{H}}} \cdot \frac{\mu \cdot n_{\mathrm{cbh}}}{\mathrm{pN_2}}\right) \tag{S7}$$

With the isotope effects of N_2 diffusion through water assumed to be negligible ($\epsilon_{\mathrm{diff}} \approx 0‰$), Eq. S7 can be simplified to the following final equation:

$$\varepsilon_{\frac{\mathrm{Norg}}{\mathrm{N2.gas}}} = \varepsilon_{\frac{\mathrm{aq}}{g}} - \varepsilon_{\mathrm{fix}} + \frac{\varepsilon_{\mathrm{fix}}}{K_1 \cdot K_{\mathrm{Y}} \cdot K_{\mathrm{H}}} \cdot \frac{\mu \cdot n_{\mathrm{cbh}}}{\mathrm{pN_2}} \tag{S8}$$

Eq. S8 was used to estimate the fractionation factor of nitrogenase ($\epsilon_{\mathrm{fix}} = -2.71 \pm 0.09‰$; Fig. 7) based on heterocyst spacing (Fig. 4), growth rate (Fig. S6) and isotopic data (Fig. 5) of *A. cylindrica* from this study, as well as literature data on $\epsilon_{\mathrm{aq/g}}$ (Fig. S11). To our knowledge, this is the first *in vivo* estimate of ϵ_{fix} for nitrogenase.

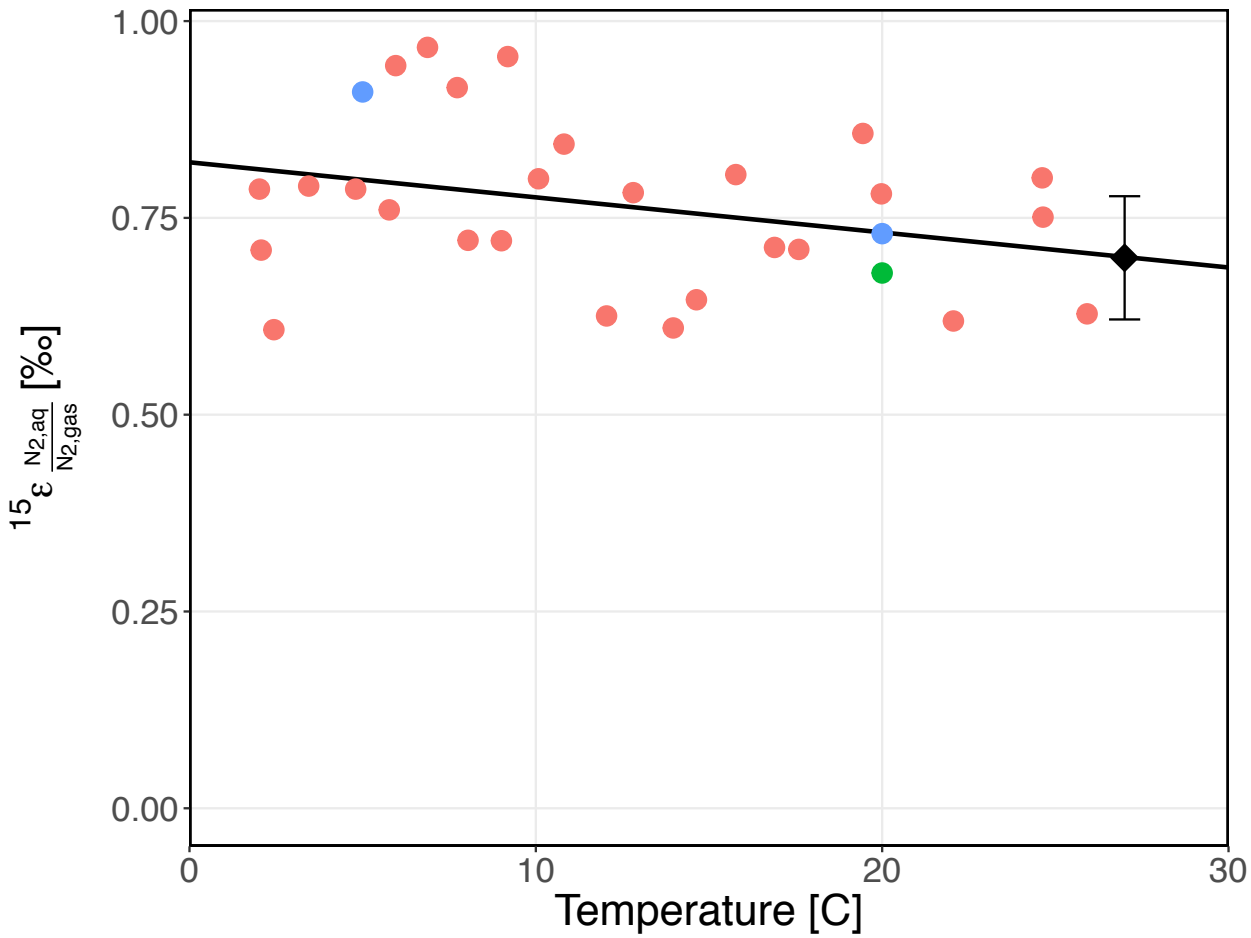

Figure S11: Temperature dependence of the equilibrium fractionation between atmospheric/headspace N_2 gas and dissolved/aqueous N_2. Diamond indicates the predicted fractionation factor ($\epsilon_{\mathrm{aq/g}} = 0.70 \pm 0.08‰$) at the growth temperature used in this study (27°C). Red data points are digitized from Fig. 1 in Klots and Benson, 1963; blue data points from Table 1 in Lee et al., 2015; and green data point from Table 1 in Knox et al., 1992.

Appendix S6: Enzyme kinetics model

In addition to its role in overall flux balance and as a constraint on growth rate, the nitrogen fixation flux inside a heterocyst (ϕ_{fix}) can also be expressed with respect to the substrate-dependent rate of enzymatic catalysis with Michaelis-Menten parameters $V_{\max}$ (the maximum rate of catalysis) and K_{M} (the half-saturation constant):

$$\phi_{\text{fix}} = V_{\max} \cdot \frac{C_{\text{N2.het}}}{C_{\text{N2.het}} + K_{\mathrm{M}}} \tag{S1}$$

Combining this equation with the growth-rate dependent flux expression derived in Eq. S5 from Appendix S5: (where $\frac{n_{\text{veg}}}{n_{\text{het}}} = n_{\text{cbh}}$) yields:

$$\frac{\mu \cdot n_{\text{cbh}}}{K_{\mathrm{Y}}} = V_{\max} \cdot \frac{C_{\text{N2.het}}}{C_{\text{N2.het}} + K_{\mathrm{M}}} \tag{S2}$$

which can be solved for n_{cbh}:

$$n_{\text{cbh}} = \frac{K_{\mathrm{Y}} V_{\max}}{\mu} \cdot \frac{C_{\text{N2.het}}}{C_{\text{N2.het}} + K_{\mathrm{M}}} \tag{S3}$$

Eliminating $C_{\text{N2.het}}$ with Eq. S4 from Appendix S5: finally yields:

$$n_{\text{cbh}} = K_{\mathrm{Y}} \cdot V_{\max} \cdot \frac{\mathrm{pN_2}}{\mu} \cdot \frac{1}{\mathrm{pN_2} + \frac{\varepsilon_{\text{fix}}}{\varepsilon_{\frac{\text{aq}}{\text{g}}} - \varepsilon_{\frac{\text{Norg}}{\text{N2.gas}}}} \cdot \frac{K_{\mathrm{M}}}{K_{\mathrm{H}}}} \tag{S4}$$

Bootstrapped non-linear least squares regression fitting of Eq. S4 based on the heterocyst spacing (Fig. 4), growth rate (Fig. S6) and isotopic data (Fig. 5) from this study provides an estimate of the Michaelis-Menten half-saturation constant K_{M} (or to be precise, $K_{\mathrm{M}}/K_{\mathrm{H}}$, the half-saturation constant in pressure instead of concentration units) for nitrogenase in each phase of *A. cylindrica* culture growth (as reported in the discussion section of the main text). Our estimates fall within the scope of other literature estimates for nitrogenase (Table S6).

Table S6: Overview of Michaelis-Menten half-saturation constants for N_2 fixation by intact cells (IC) and cell-free extracts (CFX). K_{M} values reported for this study are separated by culture growth phase.

Organism	Type	K_{M} [bar N_2]	Reference
Anabaena cylindrica (early-exponential)	IC	0.12	This study
Anabaena cylindrica (late-exponential)	IC	0.12	This study
Anabaena cylindrica	IC	0.20	Ohmori and Hattori, 1972
Anabaena variabilis	IC	0.12	Jensen and Raymond, 1983
Azotobacter vinelandii	IC	0.12	Hwang and Burris, 1972
Azotobacter vinelandii	CFX	0.16	Strandberg and Wilson, 1967
Azotobacter vinelandii	CFX	0.16	Hardy and Jr. Knight, 1967

Appendix S7: References

Hardy, R. W. F., Jr. Knight, E., 1967. ATP-dependent reduction of azide and HCN by N_2-fixing enzymes of *Azotobacter vinelandii* and *Clostridium pasteurianum*. Biochimica et Biophysica Acta 139, 69–90.

Hayes, J. M., 2004. An introduction to isotopic calculations. Atomic Energy, 1–10.

Hwang, J. C., Burris, R. H., 1972. Nitrogenase-catalyzed reactions. Biochimica et Biophysica Acta 283, 339–350.

Jensen, B. B., Raymond, R. P., 1983. Direct measurements of steady-state kinetics of cyanobacterial N_2 uptake by membrane-leak mass-spectrometry and comparisons between nitrogen-fixation and acetylene-reduction. Applied and Environmental Microbiology 45, 1331–1337.

Klots, C. E., Benson, B. B., 1963. Isotope effect in solution of oxygen and nitrogen in distilled water. Journal of Chemical Physics 38, 890–892.

Knox, M., Quay, P. D., Wilbur, D., Dec. 1992. Kinetic isotopic fractionation during air-water gas transfer of O_2, N_2, CH_4, and H_2 97, 20335–20343.

Laws, E. A., Popp, B. N., Bidigare, R. R., Kennicutt, M. C., Macko, S. A., 1995. Dependence of phytoplankton carbon isotopic composition on growth rate and $[CO_2]_{aq}$: Theoretical considerations and experimental results. Geochimica et Cosmochimica Acta 59, 1131–1138.

Lee, H., Sharp, Z. D., Fischer, T. P., 2015. Kinetic nitrogen isotope fractionation between air and dissolved N_2 in water: Implications for hydrothermal systems. Geochemical Journal 49, 571–573.

Ohmori, M., Hattori, A., 1972. Effect of nitrate on nitrogen-fixation by the blue-green alga *Anabaena cylindrica*. Plant and Cell Physiology 13, 589–599.

Sander, R., 2015. Compilation of Henry's law constants (version 4.0) for water as solvent. Atmospheric Chemistry and Physics 15, 4399–4981.

Strandberg, G. W., Wilson, P. W., 1967. Molecular H_2 and the pN_2 function of *Azotobacter*. Proceedings of the National Academy of Sciences of the United States of America 58, 1404–1409.